# Discontinuous Galerkin Isogeometric Analysis of Elliptic Problems on Non-matching Interfaces

Christoph Hofer[1], Ulrich Langer[1], and Ioannis Toulopoulos[1]

[1] Johann Radon Institute for Computational and Applied Mathematics (RICAM),
Austrian Academy of Sciences

christoph.hofer@ricam.oeaw.ac.at
ulrich.langer@ricam.oeaw.ac.at

**Abstract.** We propose a discontinuous Galerkin Isogeometric Analysis method for the numerical solution of elliptic diffusion problems on decompositions into volumetric patches with non-matching interfaces. Indeed, due to an incorrect segmentation procedure, it may happen that the interfaces of adjacent subdomains don't coincide. In this way, gap regions, which are not present in the original physical domain, are created. In this paper, the gap region is considered as a subdomain of the decomposition of the computational domain and the gap boundary is taken as an interface between the gap and the subdomains. We apply a multi-domain approach and derive a subdomain variational formulation which includes interface continuity conditions and is consistent with the original variational formulation of the problem. The last formulation is further modified by deriving interface conditions without the presence of the solution in the gap. In particular, the gap terms in the interface conditions are replaced by Taylor expansions with respect the adjacent subdomain solutions. Finally, the solution of this modified problem is approximated by developing a discontinuous Galerkin Isogeometric Analysis technique. The ideas are illustrated on a model diffusion problem with discontinuous diffusion coefficients. We develop a rigorous theoretical framework for the proposed method clarifying the influence of the gap size onto the convergence of the method. The theoretical estimates are supported by numerical examples in two- and three-dimensional computational domains.

**Key words:** Elliptic diffusion problems, Heterogeneous diffusion coefficients, Isogeometric Analysis, Decompositions into volumetric patches with non-matching interfaces, Multi-patch discontinuous Galerkin method.

## 1  Introduction

In the numerical solution of many realistic problems by means of Isogeometric Analysis (IgA), the whole computational (physical) domain $\Omega$ can often not be represented by a single volume patch that is the image of the parameter domain by a single, smooth and regular B-spline or NURBS map. In this case, it is necessary to perform a decomposition of the computational domain $\Omega$ into subdomains, in other words, to describe the domain $\Omega$ by multiple patches. Typical examples are complicated 3d domains, different diffusion coefficients, or even different mathematical models in different parts of the domain. Superior B-splines (NURBS, T-spline etc) finite dimensional spaces are used, in order to construct parametrizations for these subdomains [6]. It is typical for IgA that the same basis functions are used to approximate the solution of the problem under consideration, see [11] and [3]. Despite the advantages, that B-splines (NURBS etc) offer for the parametrization of the subdomains, some serious difficulties can arise, especially, when the subdomains topologically differ a lot from a cube. The segmentation procedure, that starts from the geometrical description of the corresponding surface patches, can lead us to non-compatible parametrizations of the geometry, meaning that the parametrized interfaces of adjusting subdomains are not identical after the volume segmentation, see, e.g., [12, 18, 20] for the discussion of isogeometric segmentation pipeline. In this paper, we call a non-watertight isogeometric segmentation also non-matching interface parametrization. The result of this phenomenon is the creation of overlapping subdomains or gap regions between adjacent subdomains. Here we are interested in the later case. Indeed, it is an important issue of the IgA framework to devise a stable numerical procedure that can successfully be applied to this type of decompositions. The contribution of this paper aims at developing a multipatch discontinuous Galerkin IgA (dG IgA) technique for this case. For simplicity, we focus on the case where we have an initial decomposition of $\Omega$, which gives non-matching parametrizations of two subdomain interfaces, and a gap region, say $\Omega_g$, appears between the two adjacent subdomains. This means that the domain decomposition is

given by $\mathcal{T}_H(\Omega \setminus \overline{\Omega}_g) := \{\Omega_l, \Omega_r\}$, and $\overline{\Omega} = \overline{\Omega}_l \cup \overline{\Omega}_r \cup \overline{\Omega}_g$. The elliptic diffusion problem, that we are going to consider as model problem, has the form: find $u : \overline{\Omega} \to R$ such that

$$-\text{div}(\rho \nabla u) = f \text{ in } \Omega \quad \text{and} \quad u = u_D \text{ on } \partial\Omega, \tag{1.1}$$

where the diffusion coefficient $\rho$ is a patch-wise positive constant function, $f$ is a given source, and $u_D$ are given Dirichlet data prescribed on the boundary $\partial\Omega$ of $\Omega$. In [16] and [14], the second and third authors have studied multipatch dG IgA methods for solving model diffusion problems like (1.1). In particular, the authors considered matching interface domain decompositions which are compatible with the jump discontinuities of the coefficient $\rho$. The weak continuity conditions across the interfaces have been imposed by introducing dG numerical fluxes, see, e.g., [8] and [22]. In this way, the solution of the problem can independently be approximated in every subdomain (in the IgA frame) and non-matching grids can be employed. Here we will heavily use the results from [16] in order to build up a stable dG IgA scheme for descritizing (1.1) on decompositions with non-matching interfaces where gaps can appear.

In the present case, we only deal with subdomains belonging to $\mathcal{T}_H(\Omega \setminus \overline{\Omega}_g)$. Thus, we need to set up an equivalent problem on $\overline{\Omega} \setminus \Omega_g$. We first apply a multi-domain approach on $\overline{\Omega}_l \cup \overline{\Omega}_r \cup \overline{\Omega}_g$ and derive a variational formulation for (1.1) by performing integration by parts separately over every subdomain. Thereafter, under some regularity assumptions imposed on the weak solution of (1.1), the contributions of the volume integrals on $\Omega_g$ are removed, and we construct an equivalent variational problem on $\mathcal{T}_H(\Omega \setminus \overline{\Omega}_g)$, where only the normal fluxes $\nabla u|_{\Omega_g} \cdot n_{\partial\Omega_g}$ on $\partial\Omega_g$ exist. However, the information that is provided by the original data of the problem does not help us to explicitly determine the fluxes $\nabla u|_{\Omega_g} \cdot n_{\partial\Omega_g}$. Thus, given the regularity of $u$ in every $\Omega_i$, the normal flux terms $\nabla u_g \cdot n_{\partial\Omega_g}$ are replaced by Taylor expansions using the known values of $u$ of the neighboring subdomains of $\Omega_g$. In that way, we settle down with our variational problem, where its solution $u$ is defined only on the subdomains belonging to $\mathcal{T}_H(\Omega \setminus \overline{\Omega}_g)$, which can consequently be approximated by the B-spline spaces. We utilize this last formulation, expressed on $\mathcal{T}_H(\Omega \setminus \overline{\Omega}_g)$, for deriving the discrete dG IgA formulation. As mentioned above, we can not produce approximations to $u_g := u|_{\Omega_g}$, since the B-spline spaces are not defined on $\Omega_g$. The accuracy of the discrete solution is affected by the Taylor polynomials which depend on the gap distance, say $d_g$, which charactirizes the maximum distance of the diametrically opposite points on $\partial\Omega_g$. In fact the Taylor expansions are playing the role of a bridge for the communication between the valus of the adjacent subdomains, and will help to build up the numerical flux in the dG IgA method over the gap region. In this work, based on the results of our recent works [16, 14], we are aiming at deriving an error estimate in the classical "broken" dG-norm $\|.\|_{dG}$ for derivation of the discrete solutions from the exact solution in terms of the mesh size $h$ and the gap distance $d_g$. In particular, we will show that, if the IgA space defined on subdomains $\Omega_i$ has the approximation power $h^k$ and the gap distance is $\mathcal{O}(h^{k+\frac{1}{2}})$ (that means that the flux approximation is of $\mathcal{O}(h^k)$), then we obtain optimal convergence rate for the error in the dG norm $\|.\|_{dG}$. In the special case where the gap distance is $\mathcal{O}(h)$, we obtain a reduced discretization error of order $\mathcal{O}(h^{\frac{1}{2}})$.

We lastly mention that several techniques have recently been investigated for coupling non-matching (or non-conforming) subdomins in some weak sense. In [23] and [19], Nitsche's method have been applied to enforce weak coupling conditions along trimmed B-spline patches. In [2], the most common techniques for imposing weakly the continuity on the interfaces have been applied and tested on nonlinear elasticity problems. The numerical tests have been performed on non-matching grid parametrizations. Furthermore, mortar methods have been developed in the IgA content utilizing different B-spline degrees for the Langrange multiplier in [5]. The method has been applied for performing numerical tests on decompositions with non-matching interface parametrizations.

The paper is organized as follows. In Section 2, some notations, the weak form of the problem and the definition of the B-spline spaces are given. We further describe the gap region. In Section 3, we present the problem in $\Omega \setminus \overline{\Omega}_g$, the approximation of the normal fluxes on the $\partial\Omega_g$, and the dG IgA scheme. In the last part of this section, we estimate the remainder terms in the Taylor expansion. Section 4 is devoted to the derivation of the a priori error estimates. Finally, in Section 5, we present

numerical tests for validating the theoretical results on two- and three- dimensional test problems. The paper closes with some conclusions in Section 6.

## 2    Preliminaries, dG IgA notation and gap representation

We start with some preliminary definitions and notations. Let $\Omega$ be a bounded Lipschitz domain in $\mathbb{R}^d$, and let $\alpha = (\alpha_1, ..., \alpha_d)$ be a multi-index of non-negative integers $\alpha_1, ...,, \alpha_d$ with degree $|\alpha| = \sum_{j=1}^{d} \alpha_j$, where we are primarily interested in the cases $d = 2$ and $d = 3$. For any $\alpha$, we define the differential operator $D^\alpha = D_1^{\alpha_1} \cdots D_d^{\alpha_d}$, with $D_j = \partial/\partial x_j$, $j = 1, \ldots, d$, and $D^{(0,\ldots,0)}u = u$. For a non-negative integer $m$, let $C^m(\Omega)$ denote the space of all functions $\phi : \Omega \to \mathbb{R}$, whose partial derivatives $D^\alpha \phi$ of all orders $|\alpha| \leq m$ are continuous in $\Omega$. We denote the subset of all functions from $C^\infty(\Omega)$ with compact support in $\Omega$ by $C_0^\infty(\Omega)$ (or $\mathcal{D}(\Omega)$). Let $1 \leq p < \infty$ be fixed and $l$ be a non-negative integer. As usual, $L^p(\Omega)$ denotes the Lebesgue spaces for which $\int_\Omega |u(x)|^p \, dx < \infty$, endowed with the norm $\|u\|_{L^p(\Omega)} = \left( \int_\Omega |u(x)|^p \, dx \right)^{\frac{1}{p}}$, and $W^{l,p}(\Omega)$ is the Sobolev space, which consists of the functions $\phi : \Omega \to \mathbb{R}$ such that their weak derivatives $D^\alpha \phi$ with $|\alpha| \leq l$ belong to $L^p(\Omega)$. If $\phi \in W^{l,p}(\Omega)$, then its norm is defined by

$$\|\phi\|_{W^{l,p}(\Omega)} = \Big( \sum_{0 \leq |\alpha| \leq l} \|D^\alpha \phi\|_{L^p(\Omega)}^p \Big)^{\frac{1}{p}} \ \text{ and } \ \|\phi\|_{W^{l,\infty}(\Omega)} = \max_{0 \leq |\alpha| \leq l} \|D^\alpha \phi\|_{L^\infty(\Omega)},$$

for $1 \leq p < \infty$ and $p = \infty$, respectively. We refer to [1] for more details about Sobolev spaces.

We end this section by recalling Hölder's and Young's inequalities: for any $\epsilon$, $0 < \epsilon < \infty$, and $1 \leq p, q \leq \infty$ such that $\frac{1}{p} + \frac{1}{q} = 1$, for all $u \in L^p(\Omega)$ and $v \in L^q(\Omega)$, there holds

$$\int_\Omega uv \, dx \leq \|u\|_{L^p(\Omega)} \|v\|_{L^q(\Omega)}, \quad \int_\Omega uv \, dx \leq \frac{\epsilon}{p} \|u\|_{L^p(\Omega)}^p + \frac{\epsilon^{-\frac{q}{p}}}{q} \|v\|_{L^q(\Omega)}^q. \tag{2.1}$$

### 2.1    Weak formulation

The weak formulation of the boundary value problem (1.1) reads as follows: for given source function $f \in L^2(\Omega)$ and Dirichlet data $u_D \in W^{\frac{1}{2},2}(\partial\Omega)$, find a function $u \in W^{1,2}(\Omega)$ such that $u = u_D$ on $\partial\Omega$ and satisfies the variational identity

$$a(u, \phi) = l_f(\phi), \ \forall \phi \in W_0^{1,2}(\Omega) = \{\phi \in W^{1,2}(\Omega) : \ \phi = 0 \text{ on } \partial\Omega\}, \tag{2.2}$$

where the bilinear form $a(\cdot, \cdot)$ and the linear form $l_f(\cdot)$ are defined by

$$a(u, \phi) = \int_\Omega \rho \nabla u \nabla \phi \, dx \quad \text{and} \quad l_f(\phi) = \int_\Omega f\phi \, dx, \tag{2.3}$$

respectively. Since we assume that the diffusion coefficient $\rho \in L^\infty(\Omega)$ and uniformly positive (later we will specify this assumption for multi-patch domains), the Lax-Milgram Lemma immediately yields existence and uniqueness of the solution $u$ of our model diffusion problem (2.2). For simplicity, we only consider non-homogeneous Dirichlet boundary conditions on $\partial\Omega$. However, the analysis presented in our paper can easily be generalized to other constellations of boundary conditions which ensure existence and uniqueness such as Robin or mixed boundary conditions.

For the developing of the the convergence analysis below for the dG IgA method that we are going to propose on subdomain decompositions with gap regions, we assume that the domain $\Omega \subset \mathbb{R}^d$ consists of two subdomains $\Omega_1$ and $\Omega_2$ with common interface $F$, i.e.,

$$\overline{\Omega} = \overline{\Omega_1} \cup \overline{\Omega_2}, \quad \Omega_1 \cap \Omega_2 = \emptyset, \quad \overline{\Omega_1} \cap \overline{\Omega_2} = F. \tag{2.4}$$

For this decomposition, we use the notation $\mathcal{T}_H(\Omega) = \{\Omega_i\}_{i=1}^2$, and define the space

$$W^{l,p}(\mathcal{T}_H(\Omega)) = \{u \in L^p(\Omega) : u|_{\Omega_i} \in W^{l,p}(\Omega_i), \text{ for } i = 1, 2\}, \tag{2.5}$$

where $l \geq 0$ is an integer and $1 \leq p \leq \infty$ is real number. For the solution, we consider the following regularity assumption.

**Assumption 1** *We allow the diffusion coefficient $\rho$ to be positive and patch-wise constant, i.e., $\rho = \rho_i > 0$ constant in $\Omega_i$, $i = 1, 2$. We assume that the solution $u$ of (2.2) belongs to $V = W^{1,2}(\Omega) \cap W^{l,p}(\mathcal{T}_H(\Omega))$ with $l \geq 2$ and $p \in (\max\{1, \frac{2d}{(d+2(l-1))}\}, 2]$.*

In what follows, positive constants $c$ and $C$ appearing in inequalities are generic constants which do not depend on the mesh-size $h$. In many cases, we will indicate on what may the constants depend for an easier understanding of the proofs. Frequently, we will write $a \sim b$ meaning that $c\,a \leq b \leq C\,a$.

### 2.2  Incorrect segmentation and non-matching parametrizations

Let us suppose for the moment that we have constructed the B-spline (or NURBS) parametric space, (see next Subsection), and we start the segmentation procedure in order to calculate the control point net for every $\Omega_i$, $i = 1, 2$. Given the control net and the B-spline space we consider each of $\Omega_i$, $i = 1, 2$ as the image, of a B-spline parametrization mapping. For reasons that we will see below, we denote the two images $\Omega_l$ and $\Omega_r$ correspondingly. The domain $\Omega$ can be consequently described by means of $\Omega_l$ and $\Omega_r$. Despite the superior properties of B-spline spaces, in several cases, as for example when $\Omega_i$, $i = 1, 2$ differ topologically a lot by a cube, the previous geometric B-spline parametrizations can lead us to non-compatible parametrizations of the common interface. This means that the parametrizations of the common interface of the adjusting subdomains are not identical, see, e.g., [12]. We will call this situation a non-matching interface parametrization. The result of this phenomenon is the creation of overlapping subdomains or gap regions between $\Omega_l$ and $\Omega_r$. Here we are interested in the later case. For the purposes of this paper, it suffices to consider the case where only one gap region, say $\Omega_g$, exists between $\Omega_l$ and $\Omega_r$, and either $\Omega_l \subset \Omega_1$ or $\Omega_r \subset \Omega_2$. As an immediate result we have that $\overline{\Omega} = \overline{\Omega}_l \cup \overline{\Omega}_g \cup \overline{\Omega}_r$, see an illustration in Fig. 2(c). In what follows, we will call $\Omega_l$ and $\Omega_r$ parametrized subdomains or simply subdomains, if there is no chance of confusion with $\Omega_i$, $i = 1, 2$. We denote by $\mathcal{T}_H(\Omega \setminus \overline{\Omega}_g) = \{\Omega_l, \Omega_r\}$.

In Fig. 1, we illustrate a general two-dimensional case, where more than two subdomains do not match parametrically on the internal interfaces.[1]



(a)                                                         (b)

**Fig. 1.** (a) A geometric illustration of a decomposition including gap regions between the adjacent subdomains, (b) The decomposition without any gap region.

### 2.3  B-spline spaces

In this section, we briefly present the B-spline spaces and the form of the B-spline parametrizations for the physical subdomains. For a more detailed presentation we refer to [6], [7], [24].

Let us consider the unit cube $\widehat{\Omega} = (0,1)^d \subset \mathbb{R}^d$, which we will refer to as the parametric domain and let $\overline{\Omega} = \bigcup_{i=1}^{N} \overline{\Omega}_i$, with $\Omega_i \cap \Omega_j = \emptyset$, for $i \neq j$ be a decomposition of $\Omega$. Let the integers $k$,

---

[1] The two figures have been provided by the Institute of Applied Geometry of Johannes Kepler University of Linz.

$i = 1, ..., N$ and $n_\iota$, $\iota = 1, ..., d$ denote the given B-spline degree, the coresponding physical $i - th$ subdomain, and the number of basis functions of the B-spline space that will be constructed in $x_\iota$-direction. We introduce the $d-$dimensioanl vector of knots $\mathbf{\Xi}_i^d = (\Xi_i^1, ..., \Xi_i^\iota, ..., \Xi_i^d)$, $\iota = 1, ..., d$, with the particular components given by $\Xi_i^\iota = \{0 = \xi_1^\iota \leq \xi_2^\iota \leq ... \leq \xi_{n_\iota+k+1}^\iota = 1\}$. The components $\Xi_i^\iota$ of $\mathbf{\Xi}_i^d$ form a mesh $T_{h_i,\widehat{\Omega}}^{(i)} = \{\hat{E}_m\}_{m=1}^{M_i}$ in $\widehat{\Omega}$, where $\hat{E}_m$ are the micro elements and $h_i$ is the mesh size, which is defined as follows. Given a micro element $\hat{E}_m \in T_{h_i,\widehat{\Omega}}^{(i)}$, we set $h_{\hat{E}_m} = diameter(\hat{E}_m) = \max_{x_1,x_2 \in \bar{\hat{E}}_m} \|x_1 - x_2\|_d$, where $\|.\|_d$ is the Euclidean norm in $\mathbb{R}^d$ and the subdomain mesh size $h_i$ is defined to be $h_i = \max\{h_{\hat{E}_m}\}$. We define $h = \max_{i=1,...,N}\{h_i\}$.

**Assumption 2** *The meshes $T_{h_i,\widehat{\Omega}}^{(i)}$ are quasi-uniform, i.e., there exist a constant $\theta \geq 1$ such that $\theta^{-1} \leq h_{\hat{E}_m}/h_{\hat{E}_{m+1}} \leq \theta$. Also, we assume that $h_i \sim h_j$ for $i \neq j$.*

Given the knot vector $\Xi_i^\iota$ in every direction $\iota = 1, ..., d$, we construct the associated univariate B-spline functions, $\hat{\mathbb{B}}_{\Xi_i^\iota,k} = \{\hat{B}_{1,\iota}^{(i)}(\hat{x}_\iota), ..., \hat{B}_{n_\iota,\iota}^{(i)}(\hat{x}_\iota)\}$ using the Cox-de Boor recursion formula, see details in [6], [7]. On the mesh $T_{h_i,\widehat{\Omega}}^{(i)}$, we define the multivariant B-spline space, $\hat{\mathbb{B}}_{\mathbf{\Xi}_i^d,k}$, to be the tensor-product of the coresponding univariate $\mathbb{B}_{\Xi_i^\iota,k}$ spaces. Accordingly, the B-spline functions of $\hat{\mathbb{B}}_{\mathbf{\Xi}_i^d,k}$ are defined by the tensor-product of the univariante B-spline basis functions, that is

$$\hat{\mathbb{B}}_{\mathbf{\Xi}_i^d,k} = \otimes_{\iota=1}^d \hat{\mathbb{B}}_{\Xi_i^\iota,k} = span\{\hat{B}_j^{(i)}(\hat{x})\}_{j=1}^{n=n_1 \times ... \times n_\iota \times ... \times n_d}, \tag{2.6}$$

where each $\hat{B}_j^{(i)}(\hat{x})$ has the form

$$\hat{B}_j^{(i)}(\hat{x}) = \hat{B}_{j_1}^{(i)}(\hat{x}_1) \times ... \times \hat{B}_{j_\iota}^{(i)}(\hat{x}_\iota) \times ... \times \hat{B}_{j_d}^{(i)}(\hat{x}_d), \text{ with } \hat{B}_{j_\iota}^{(i)}(\hat{x}_\iota) \in \hat{\mathbb{B}}_{\Xi_i^\iota,k}. \tag{2.7}$$

Finally, having the B-spline spaces and the B-spline control points $C_j^{(i)}$, we can represent each subdomain $\Omega_i$, $i = 1, ..., N$ by the parametric mapping

$$\mathbf{\Phi}_i : \widehat{\Omega} \to \Omega_i, \quad x = \mathbf{\Phi}_i(\hat{x}) = \sum_{j=1}^n C_j^{(i)} \hat{B}_j^{(i)}(\hat{x}) \in \Omega_i, \tag{2.8}$$

where $\hat{x} = \mathbf{\Psi}_i(x) := \mathbf{\Phi}_i^{-1}(x)$, cf. [6].

We construct a mesh $T_{h_i,\Omega_i}^{(i)} = \{E_m\}_{m=1}^{M_i}$ for every $\Omega_i$, whose vertices are the images of the vertices of the corresponding parametric mesh $T_{h_i,\widehat{\Omega}}^{(i)}$ through $\mathbf{\Phi}_i$. For each $E \in T_{h_i,\Omega_i}^{(i)}$, we denote its support extension by $D_E^{(i)}$, where the support extension is defined to be the interior of the set formed by the union of the supports of all B-spline functions whose supports intersects $E$.

For $i = 1, ..., N$, we construct the B-spline space $\mathbb{B}_{\mathbf{\Xi}_i^d,k}$ on $\Omega_i$ by

$$\mathbb{B}_{\mathbf{\Xi}_i^d,k} := \{B_j^{(i)}|_{\Omega_i} : B_j^{(i)}(x) = \hat{B}_j^{(i)} \circ \mathbf{\Psi}_i(x), \text{ for } \hat{B}_j^{(i)} \in \hat{\mathbb{B}}_{\mathbf{\Xi}_i^d,k}\}. \tag{2.9}$$

The global B-spline space $V_h$ with components on every $\mathbb{B}_{\mathbf{\Xi}_i^d,k}$ is defined by

$$V_h := V_{h_1} \times ... \times V_{h_N} := \mathbb{B}_{\mathbf{\Xi}_1^d,k} \times ... \times \mathbb{B}_{\mathbf{\Xi}_N^d,k}. \tag{2.10}$$

We refer the reader to [6] for more information about the meaning of the knot vectors in CAD and IgA.

*Remark 1.* The B-spline spaces presented above are referred to the general case of $N$ subdomains. In this paper, for the sake of simplicity, we assume that we have $N = 2$. The mappings in (2.8) produce (and are referred to) matching interface parametrizations. Throughout the paper it is understood that we study the case where the mappings in (2.8) produce non-matching interface parametrizations and a gap region appears between the adjacent subdomians, see Section 2.2.

**Assumption 3** *We assume that $k \geq l$, cf. Assumption 1.*
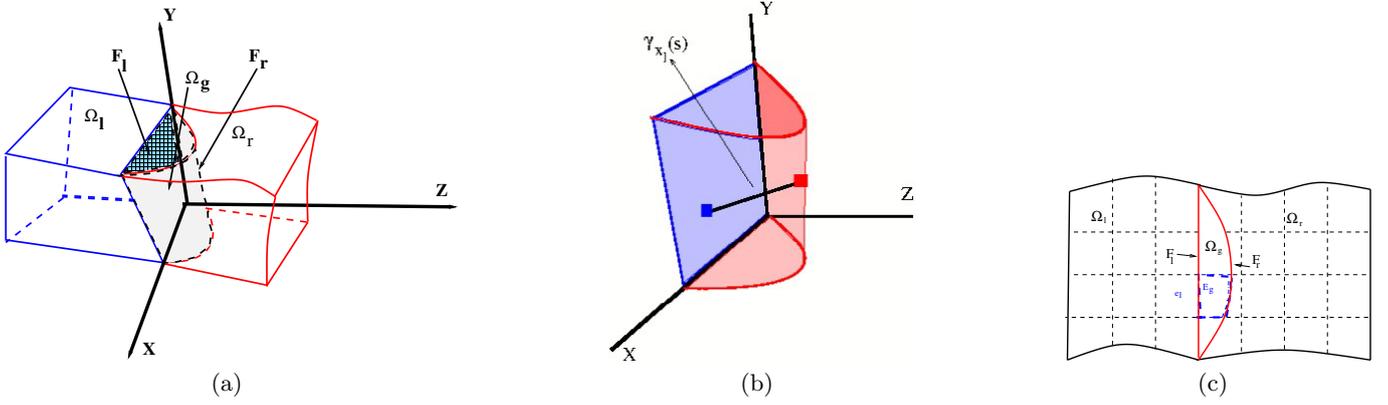
**Fig. 2.** (a) Illustration of the gap region between two adjacent sub domains in $d = 3$ case, (b) the diametrically opposite points located on $\partial \Omega_g$ in $d = 3$ case, (c) an illustration for the $d = 2$ case.

### 2.4   The gap region

Let us now suppose that $\Phi_l : \widehat{\Omega} \to \Omega_l$ and $\Phi_r : \widehat{\Omega} \to \Omega_r$ are two parametrization mappings that give a non-matching interface parametrization. Let $\Omega_g$, be the gap region between $\Omega_l$ and $\Omega_r$ and let us consider that $\partial \Omega_g = F_l \cup F_r$ with $F_l \subset \partial \Omega_l$ and $F_r \subset \partial \Omega_r$, see Figs. 2(a) and 2(c). We further assume that there is a $h_0$ such that

$$\Omega_1 = \Omega_l, \quad \Omega_g \subset \Omega_2, \quad \text{and} \quad \overline{\Omega}_2 = \overline{\Omega}_g \cup \overline{\Omega}_r, \quad \forall h \le h_0, \tag{2.11}$$

which implies that $F_l := F$, see (2.4). For simplicity, $F_l$ is considered to be a simple region, and it can be described as the set of points $(x, y, z)$ satisfying

$$0 \le y \le y_M, \ \psi_1(y) \le x \le \psi_2(y), \ z = 0, \tag{2.12}$$

where $y_M$ is a fixed real number and $\psi_i$ with $i = 1, 2$ are given continuous functions. An illustration is shown in Fig. 2(b). Our next goal is to assign the points $x_l \in F_l$ to the points of the other face $x_r \in F_r$, in order to build up later the numerical flux function. The assignment between the opposite points is achieved by considering $F_r$ as a graph of a B-spline function $\zeta_0(x_{l,1}, x_{l,2})$. In particular, having the description (2.12) for $F_l$ with unit normal vector $n_{F_l} = (0, 0, 1)$, we construct a parametrization $\Phi_{l,r} : F_l \to F_r$ for $F_r$ of the form

$$\Phi_{l,r}(x_l) = x_l + \zeta_0(x_l) n_{F_l} := x_r \in F_r, \tag{2.13}$$

or more analytically

$$F_r = \{ x_r : (x_{r,1} = x_{l,1}, x_{r,2} = x_{l,2}, x_{r,3} = x_{l,3} + \zeta_0(x_l)) \}, \tag{2.14}$$

where the B-spline $\zeta_0$ function is determined by $\Phi_r|_{F_r}$. We define the corresponding mapping $\Phi_{r,l} : F_r \to F_l$ to be the projection of the $F_r$ graph onto $xy-$plane, that is

$$\Phi_{r,l}(x_r) = (x_{l,1}, x_{l,2}, 0), \quad \text{where} \quad \Phi_{l,r}(x_{l,1}, x_{l,2}, 0) = x_r. \tag{2.15}$$

We will see later that the parametrization mapping (2.15) simplifies the analysis and is convenient for performing the numerical tests.

*Remark 2.* One could consider a mapping $\Phi_{r,l} : F_r \to F_l$ having the same form as the mapping $\Phi_{l,r}$, e.g. $\Phi_{r,l} = x_r + \tilde{\zeta}_0(x_r) n_{F_r} := x_l^* \in F_l$, where $n_{F_r}$ is the normal vector on $F_r$ inward to $\Omega_g$. In this case, the point $x_l^*$ is different (in general) from the original point $x_l = x_r - \zeta_0(x_l) n_{F_l}$ used in (2.13) and this seems to make the analysis more complicated. This is because, when we will construct later the numerical flux on $F_l$ and on $F_r$, we have to take into account two different assignments of the diametrically opposite points $x_l$ and $x_r$. As we will see later using a parametrization mapping as

in (2.15) simplifies a lot the analysis and helps on an easy materialization of the method. We note further, that we have to take into account the two coresponding outward normals, i.e., the $n_{F_l}$ on $F_l$ and $n_{F_r}$ on $F_r$. The consideration of the general vector $n_{F_r}$ on $F_r$, causes rather further technical difficulties in the numerical computations. Since we are indending to develop a method that can be easily materialized for practical applications and having in our mind a small gap regions, see few lines below (2.18), we suppose that the angle formed between $n_{F_l}$ and $-n_{F_r}$ is almost zero, that is $\cos \sphericalangle(n_{F_l}, -n_{F_r}) \approx 1$.

We finally characterize the points which belong in the interval $[x_l, x_r]$. To this end, for every $x_l \in F_l$ we construct a $C^1$ one-to-one map $\gamma_{x_l} : [0, 1] \to \overline{\Omega}_g$,

$$\gamma_{x_l}(s) = x_l + s(x_r - x_l), \quad \text{with} \quad \mathbf{\Phi}_{l,r}(x_l) = x_r. \tag{2.16}$$

The function $\gamma_{x_l}$ help us to quantify the size of the gap by introducing the gap distance defined by

$$d_g = \max_{x_l}\{|\gamma_{x_l}(0) - \gamma_{x_l}(1)|\}. \tag{2.17}$$

Of special interest in our analysis are gap regions whose distance decreases polynomially in $h$.

**Assumption 4** *We assume that for any $h \leq h_0$, see (2.11), holds*

$$d_g \leq h^\lambda, \quad with \quad \lambda \geq 1. \tag{2.18}$$

Finally, based on the previous properties of the shape of $\Omega_g$, without loss of generality, we can assume that the parametrization $\mathbf{\Phi}_{l,r}$ in (2.13) has the form

$$\mathbf{\Phi}_{l,r}(x_l) = x_l + d_g\, \zeta(x_l) n_{F_l}, \quad x_l \in F_l, \tag{2.19}$$

where $\zeta$ is a B-spline and $\|\zeta\|_{L^\infty} = 1$. In Section 5 *Numerical tests*, we give explicitly the form of the mapping $\mathbf{\Phi}_{l,r}$.

**Properties of the parametrization mappings** Let us denote by $D\mathbf{\Phi}_{l,r}(x_l)$ the Jacobian matrix of $\mathbf{\Phi}_{l,r}(x_l)$ evaluated at $x_l = (x_{l,1}, x_{l,2}, x_{l,3}) \in F_l$ and by $D^\top\mathbf{\Phi}_{l,r}(x_l)$ its transpose. By an application of the chain rule we can verify that

$$\nabla(u \circ \mathbf{\Phi}_{l,r}(x_l)) = D^\top\mathbf{\Phi}_{l,r}(x_l)(\nabla u) \circ \mathbf{\Phi}_{l,r}(x_l). \tag{2.20}$$

If $u$ is a function defined on the prametrized surface $F_r$ then holds

$$\int_{F_r} u\, dF_r = \int_{F_l} u(\mathbf{\Phi}_{l,r}(x_l))J\, dx_l, \tag{2.21a}$$

$$\int_{F_r} \nabla u \cdot n_{F_l}\, dF_r = \int_{F_l} D^\top\mathbf{\Phi}_{l,r}(x_l)(\nabla u) \circ \mathbf{\Phi}_{l,r}(x_l) \cdot n_{F_l} J\, dx_l, \tag{2.21b}$$

where $J = \sqrt{(d_g\zeta_{x_{l,1}})^2 + (d_g\zeta_{x_{l,2}})^2 + 1}$ is the norm of the outward normal vector on $F_r$.

## 2.5 Jumps and $\|.\|_{dG}$

For the face $F_i$, $i = l, r$, let $n_{F_i}$ be its unit normal vector towards $\Omega_g$. For a smooth function $\phi$ defined on $\Omega$, we define its interface averages and the jumps as

$$[\![\phi]\!]|_{F_i} = \left(\phi_i - \phi_g\right), \qquad \{\phi\}|_{F_i} = \frac{1}{2}\left(\phi_i + \phi_g\right), \tag{2.22}$$

$$[\![\rho\nabla\phi]\!]|_{F_i} \cdot n_{F_i} = \left(\rho_i\nabla\phi_i - \rho_g\nabla\phi_g\right) \cdot n_{F_i}, \qquad \{\rho\nabla\phi\}|_{F_i} \cdot n_{F_i} = \frac{1}{2}\left(\rho_i\nabla\phi_i + \rho_g\nabla\phi_g\right) \cdot n_{F_i}.$$

Based on Assumption 1, we can infer that the exact solution satisfies

$$[\![u]\!]|_F = 0, \quad \text{and} \quad [\![\rho \nabla u]\!]|_F = 0. \tag{2.23}$$

To proceed to our analysis, we need to define the broken dG-norm, $\|.\|_{dG}$. For $v \in V + V_h$, we define

$$\|v\|_{dG}^2 = \sum_{i=l,r} \left( \rho_i \|\nabla v_i\|_{L^2(\Omega_i)}^2 + \frac{\rho_i}{h} \|v_i\|_{L^2(\partial\Omega_i \cap \partial\Omega)}^2 + \frac{\{\rho\}}{h} \|v_i\|_{L^2(F_i)}^2 \right), \tag{2.24}$$

Next, we show that the values of the exact solution $u$ on the opposite assigned points will coincide as $d_g \to 0$.

**Proposition 1.** *Let the Assumption 1 and (2.18) hold true. For $x_l \in F_l$, let $x_r \in F_r$ be its corresponding assigned point. Then for $\phi \in \mathcal{D}(\Omega)$ we have*

$$\left| \int_{F_l} (u(x_l) - u(x_r))\phi(x_l) \, dx_l \right| \xrightarrow{d_g \to 0} 0. \tag{2.25}$$

*Proof.* By Assumption 1 it follows that

$$\left| \int_{F_l} (u(x_l) - u(x_r))\phi(x_l) \, dx_l \right| = \left| \int_{F_l} \phi(x_l) \int_0^1 \frac{d}{ds} u(x_l + s(x_r - x_l)) \, ds \, dx_l \right|$$

$$\leq \int_{F_l} \int_0^1 |\phi(x_l)| |x_l - x_r| |Du(x_l + s(x_r - x_l))| \, ds \, dx_l. \tag{2.26}$$

Since $0 \leq s \leq 1$ the values of $z = x_l + s(x_r - x_l)$ are restricted in $\Omega_g \subset \Omega_2$ and the integration domain $F_l \times [0,1] \subseteq \Omega_2$. Henceforth, applying (2.1), in (2.26) we get the estimate

$$\left| \int_{F_l} (u(x_l) - u(x_r))\phi(x_l) \, dx_l \right| \leq d_g \|\phi\|_{L^p(\Omega_2)} \|Du\|_{L^p(\Omega_2)}, \tag{2.27}$$

that proves (2.25). $\blacksquare$

## 3   The problem on $\Omega \setminus \overline{\Omega}_g$

The next goal is to derive a variational problem in $\Omega \setminus \overline{\Omega}_g$, such that its (unique) solution on the subdomains $\Omega_i$, $i = l, r$ coincides with the solution of (2.2). The bilinear form of this problem will be determined by taking into account the normal fluxes on $\partial\Omega_g$. Finally, the problem will be discretized by dG IgA methods. The main importance is to devise appropriate numerical fluxes, which will use the diametrically opposite assigned values of $\nabla u$ and $u$ on $\partial\Omega_g$.

Recall that $\overline{\Omega} = \overline{\Omega_l} \cup \overline{\Omega_g} \cup \overline{\Omega_r}$. Now, multiplying (1.1) by a $\phi \in C_0^\infty(\Omega)$, integrating on every $\Omega_i$ separately, then performing integration by parts, and finally summing over all $\Omega_i$, $i = l, g, r$, we get

$$\int_{\Omega_l} \rho \nabla u \cdot \nabla \phi \, dx - \int_{\partial\Omega_l \cap \partial\Omega} \rho \nabla u \cdot n_{\partial\Omega_l} \phi \, d\sigma$$

$$+ \int_{\Omega_g} \rho \nabla u \cdot \nabla \phi \, dx - \int_{F_l} [\![\rho \nabla u \phi]\!] \cdot n_{F_l} \, d\sigma - \int_{F_r} [\![\rho \nabla u \phi]\!] \cdot n_{F_r} \, d\sigma$$

$$+ \int_{\Omega_r} \rho \nabla u \cdot \nabla \phi \, dx - \int_{\partial\Omega_r \cap \partial\Omega} \rho \nabla u \cdot n_{\partial\Omega_r} \phi \, d\sigma = \sum_i \int_{\Omega_i} f\phi \, dx. \tag{3.1}$$

Applying the equality $[\![\rho\nabla u\phi]\!] = \{\rho\nabla u\}[\![\phi]\!] + [\![\rho\nabla u]\!]\{\phi\}$ in (3.1), and using $\int [\![\rho\nabla u]\!] \cdot n_{\partial\Omega_g}\{\phi\}\, d\sigma = 0$, we obtain

$$
\int_{\Omega_l} \rho\nabla u \cdot \nabla\phi\, dx - \int_{\partial\Omega_l \cap \partial\Omega} \rho\nabla u \cdot n_{\partial\Omega_l}\phi\, d\sigma - \int_{F_l} \{\rho\nabla u\} \cdot n_{F_l}[\![\phi]\!]\, d\sigma
$$
$$
- \int_{\Omega_g} \mathrm{div}(\rho\nabla u)\phi\, dx - \int_{F_l} \{\rho\nabla u\} \cdot n_{F_l}\phi\, d\sigma - \int_{F_r} \{\rho\nabla u\} \cdot n_{F_r}\phi\, d\sigma
$$
$$
+ \int_{\Omega_r} \rho\nabla u \cdot \nabla\phi\, dx - \int_{\partial\Omega_r \cap \partial\Omega} \rho\nabla u \cdot n_{\partial\Omega_r}\phi\, d\sigma - \int_{F_r} \{\rho\nabla u\} \cdot n_{F_r}[\![\phi]\!]\, d\sigma
$$
$$
= \int_{\Omega\setminus\Omega_g} f\phi\, dx + \int_{\Omega_g} f\phi\, dx, \quad (3.2)
$$

where we applied an integration by parts formula on $\Omega_g$ and used $\int_{F_i} \rho_g\nabla u_g \cdot n_{\partial\Omega_g}\phi\, d\sigma = \frac{1}{2}\int_{F_i}(\rho_g\nabla u_g + \rho_i\nabla u_i) \cdot n_{\partial\Omega_g}\phi\, d\sigma$ for $i = l, r$. Finally, by (2.2), we have

$$
\int_{\Omega_l} \rho_l\nabla u \cdot \nabla\phi\, dx - \int_{\partial\Omega_l \cap \partial\Omega} \rho_l\nabla u \cdot n_{\partial\Omega_l}\phi\, d\sigma - \int_{F_l} \{\rho\nabla u\} \cdot n_{F_l}\phi\, d\sigma
$$
$$
+ \int_{\Omega_r} \rho_r\nabla u \cdot \nabla\phi\, dx - \int_{\partial\Omega_r \cap \partial\Omega} \rho_r\nabla u \cdot n_{\partial\Omega_r}\phi\, d\sigma - \int_{F_r} \{\rho\nabla u\} \cdot n_{F_r}\phi\, d\sigma
$$
$$
= \int_{\Omega\setminus\overline{\Omega}_g} f\phi\, dx, \quad \text{for all} \quad \phi \in C_0^\infty(\Omega). \quad (3.3)
$$

Evidently, solution $u$ of (2.2) satisfies (3.3) under Assumption 1.

Let $u \in V \cap W^{2,2}(\mathcal{T}_H(\Omega))$. We introduce the space

$$
V_{0,\partial\Omega} := \{v \in W^{1,2}(\Omega_l) \cup W^{1,2}(\Omega_r)\,|v = 0 \text{ on } \partial\Omega_1 \cap \partial\Omega \text{ and } \partial\Omega_2 \cap \partial\Omega\}. \quad (3.4)
$$

By the preceding analysis, we settle down the following problem: find $\hat{u} \in W^{1,2}(\Omega_l \cup \Omega_r)$ and $\hat{u} := u_D$ on $\partial\Omega$ such that

$$
a_{\setminus\Omega_g}(\hat{u}, v) = l_{f,\setminus\Omega_g}(v) + l_{\nabla u_g}(v), \quad v \in V_{0,\partial\Omega}, \quad (3.5)
$$

where the forms are defined by

$$
a_{\setminus\Omega_g}(\hat{u}, v) = \int_{\Omega_l \cup \Omega_r} \rho\nabla\hat{u} \cdot \nabla v\, dx, \quad (3.6)
$$
$$
l_{f,\setminus\Omega_g}(v) + l_{\nabla u_g}(v) = \int_{\Omega_l \cup \Omega_r} fv\, dx + \int_{\partial\Omega_g} \rho_g\nabla u_g \cdot n_{\partial\Omega_g}v\, d\sigma. \quad (3.7)
$$

Since $f \in L^2(\Omega)$ and $\rho\nabla u_g \cdot n_{\partial\Omega_g} \in L^2(\partial\Omega_g)$, Lax-Milgram Lemma ensures that problem (3.5) has a unique solution. Note that, for this case, the solution $u$ of (2.2) satisfies problem (3.5). Therefore, $\hat{u}$ coincides with $u$.

We return to the relation (3.3), which will be the basis for the definition of the numerical scheme. The normal flux terms $\nabla u_g \cdot n_{\partial\Omega_g}$, which appear in (3.3), e.g., $\int_{F_l}\{\rho\nabla u\} \cdot n_{F_l}\phi\, d\sigma = \int_{F_l} \frac{1}{2}(\rho_l\nabla u_l + \rho_g\nabla u_g) \cdot n_{F_l}\phi\, d\sigma$, are still unknown, in the sense that their values are not predefined for an explicit use in the computations. Next, Taylor expansions are used for approximating these normal fluxes.

*Remark 3.* To check consistency properties, we replace in (3.3) the $\phi$ by $\phi_h \in V_h$ and integrate by parts on each $\Omega_i, i = l, r$ to get

$$
\sum_{i=l,r}\int_{\Omega_i} \rho_i\nabla u \cdot \nabla\phi_h\, dx - \sum_{i=l,r}\int_{\partial\Omega_i \cap \partial\Omega} \rho_i\nabla u \cdot n_{\partial\Omega_i}\phi_h\, d\sigma - \sum_{i=l,r}\int_{F_i} \{\rho\nabla u\} \cdot n_{F_i}\phi_h\, d\sigma
$$
$$
= -\sum_{i=l,r}\int_{\Omega_i} \mathrm{div}(\rho\nabla u)\phi_h\, dx = \int_{\Omega\setminus\overline{\Omega}_g} f\phi_h\, dx. \quad (3.8)
$$

### 3.1   Approximating the normal fluxes $\nabla u_g \cdot n_{\partial \Omega_g}$

Our goal in the present paragraph is to use Taylor theorem for constructing approximations of $\rho_g \nabla u_g \cdot n_{\partial \Omega_g}|_{\partial \Omega_g}$. The central idea is to apply the Taylor theorem along the lines $\gamma_{x_l}$ (or $\gamma_{x_r}$), see (2.16), emanating from $x_l$ (or $x_r$) and heading in the direction of the diametrically opposite point $x_r$ (or $x_l$ correspondingly). In that way, we produce approximations of $\rho_g \nabla u_g \cdot n_{\partial \Omega_g}|_{\partial \Omega_g}$ using $u_l$ and $u_r$.

We recall the following Taylor's formula with integral remainder, for $f \in C^m([0,1])$

$$f(1) = f(0) + \sum_{j=1}^{m-1} \frac{1}{j!} f^{(j)}(0) + \frac{1}{(m-1)!} \int_0^1 s^{m-1} f^{(m)}(1-s)\,ds. \tag{3.9}$$

Let us suppose for the moment that $u \in C^m(\Omega)$. As usual, let $x_l = (x_{l,1}, x_{l,2}, x_{l,3})$ be a fixed point on $F_l$ and $x_r = \Phi_{l,r}(x_l)$. We define $f(s) = u(\gamma_{x_l}(s)) = u(x_l + s(x_r - x_l))$. By chain rule we can obtain

$$f^{(j)}(s) = \sum_{|\alpha|=j} \frac{j!}{\alpha!} D^\alpha u(x_l + s(x_r - x_l))(x_r - x_l)^\alpha, \tag{3.10}$$

where $\alpha! = \alpha_1!...\alpha_d!$ and $(x_r - x_l)^\alpha = (x_{r,1} - x_{l,1})^{\alpha_1}...(x_{r,d} - x_{l,d})^{\alpha_d}$. Combining (3.9) and (3.10), we obtain

$$u(x_r) = u(x_l) + \sum_{0<|\alpha|<m} \frac{1}{\alpha!} D^\alpha u(x_l)(x_r - x_l)^\alpha + \sum_{|\alpha|=m} (x_r - x_l)^\alpha \frac{m}{\alpha!} \int_0^1 s^{m-1} D^\alpha u(x_r + s(x_l - x_r))\,ds. \tag{3.11}$$

Setting $m = 2$ in (3.11), we get

$$u(x_r) = u(x_l) + \nabla u(x_l) \cdot (x_r - x_l) + Ru(x_l), \tag{3.12a}$$

where

$$Ru(x_l) = \sum_{|\alpha|=2} (x_r - x_l)^\alpha \frac{2}{\alpha!} \int_0^1 s D^\alpha u(x_r + s(x_l - x_r))\,ds. \tag{3.12b}$$

Now, we use (3.12) to approximate the flux terms $\nabla u_g \cdot n_{F_l}$ in (3.3). Denoting $r_l = x_r - x_l$ and $r_r = -r_l$, by (2.19) we conclude that $n_{F_l} = \frac{r_l}{|r_l|}$ and $n_{F_r} = \frac{r_r}{|r_r|}$. Using that $0 = [\![u]\!]|_{F_l} = (u_l(x_l) - u_g(x_l))$ and (3.12), we have

$$u_r(x_r) = u_g(x_l) + \nabla u_g(x_l) \cdot r_l + Ru_g(x_l) \tag{3.13a}$$
$$u_g(x_l) = u_r(x_r) - \nabla u_r(x_r) \cdot r_l + Ru_r(x_r), \tag{3.13b}$$

and we can find that

$$\nabla u_g \cdot n_{F_l} = \nabla u_r \cdot n_{F_l} - \frac{1}{|r_l|}(Ru_r(x_r) + Ru_g(x_l)) \tag{3.14a}$$

$$-\frac{1}{h}(u_l(x_l) - u_r(x_r)) = \frac{|r_l|}{h} \nabla u_g(x_l) \cdot n_{F_l} + \frac{1}{h} Ru_g(x_l). \tag{3.14b}$$

Next, we adopt the notations

$$u_l := u_l(x_l), \ u_r := u_r(x_r), \ x_r = \Phi_{l,r}(x_l)),$$

$$Ru_g(x_r + s(x_l - x_r)) := \sum_{|\alpha|=2} (x_r - x_l)^\alpha \frac{2}{\alpha!} \int_0^1 s D^\alpha u(x_r + s(x_l - x_r))\,d\sigma,$$

$$Ru_r(x_l + s(x_r - x_l)) := \sum_{|\alpha|=2} (x_l - x_r)^\alpha \frac{2}{\alpha!} \int_0^1 s D^\alpha u(x_l + s(x_r - x_l))\,d\sigma.$$

For $\phi_h \in V_h$, it follows by (3.14) that

$$\int_{F_l} \left(\frac{\rho_l}{2}\nabla u_l + \frac{\rho_g}{2}\nabla u_g\right) \cdot n_{F_l}\phi_h - \frac{\{\rho\}}{h}[\![u]\!]\phi_h \, d\sigma =$$

$$\int_{F_l} \frac{\rho_l}{2}\nabla u_l \cdot n_{F_l}\phi_h + \frac{\rho_g}{2}\nabla u_r \cdot n_{F_l}\phi_h - \left(\frac{\rho_g}{2|r_l|}Ru_g(x_r + s(x_l - x_r)) + \frac{\rho_g}{2|r_l|}Ru_r(x_l + s(x_r - x_l))\right)\phi_h$$

$$-\frac{\{\rho\}}{h}(u_l - u_r)\phi_h + \frac{\{\rho\}}{h}\left(|r_l|\nabla u_g \cdot n_{F_l} + Ru_g(x_r + s(x_l - x_r))\right)\phi_h \, d\sigma =$$

$$\int_{F_l}\left(\frac{\rho_l}{2}\nabla u_l + \frac{\rho_g}{2}\nabla u_r\right) \cdot n_{F_l}\phi_h - \frac{\{\rho\}}{h}(u_l - u_r)\phi_h \, d\sigma -$$

$$\int_{F_l}\left(\frac{\rho_g}{2|r_l|}Ru_g(x_r + s(x_l - x_r)) + \frac{\rho_g}{2|r_l|}Ru_r(x_l + s(x_r - x_l))\right)\phi_h \, d\sigma +$$

$$\int_{F_l}\frac{\{\rho\}}{h}\left(|r_l|\nabla u_g \cdot n_{F_l} + Ru_g(x_r + s(x_l - x_r))\right)\phi_h \, d\sigma. \quad (3.15)$$

Using that $[\![\rho\nabla u]\!]|_{F_i} = 0$ for $i = l, r$, the assumption that $\cos \sphericalangle(n_{F_l}, -n_{F_r}) \approx 1$, relations (2.21), definition (2.15) and relations (3.13) and (3.14), we can derive the corresponding form for the second flux term on $F_r$

$$\int_{F_r}\left(\frac{\rho_r}{2}\nabla u_r + \frac{\rho_g}{2}\nabla u_g\right) \cdot n_{F_r}\phi_h - \frac{\{\rho\}}{h}[\![u]\!]\phi_h \, d\sigma =$$

$$\int_{F_r}\left(\frac{\rho_r}{2}\nabla u_r + \frac{\rho_l}{2}\nabla u_l\right) \cdot n_{F_r}\phi_h - \frac{\{\rho\}}{h}(u_r - u_l)\phi_h \, d\sigma -$$

$$\int_{F_r}\left(\frac{\rho_g}{2|r_r|}Ru_g(x_l + s(x_r - x_l)) + \frac{\rho_g}{2|r_r|}Ru_l(x_r + s(x_l - x_r))\right)\phi_h \, d\sigma +$$

$$\int_{F_r}\frac{\{\rho\}}{h}\left(|r_r|\nabla u_g \cdot n_{F_r} + Ru_g(x_l + s(x_r - x_l))\right)\phi_h \, d\sigma. \quad (3.16)$$

*Remark 4.* We point out that in general holds $n_{F_r}|_{F_r} \neq -n_{F_l}$ and based on (2.20) and (2.21), we get

$$\int_{F_l}\rho_r D^{-\top}\nabla u_r(\mathbf{\Phi}_{l,r}(x_l)) \cdot (-n_{F_l})J \, dx_l \neq \int_{F_l}\rho_r D^{-\top}\nabla u_r(\mathbf{\Phi}_{l,r}(x_l)) \cdot n_{F_r}J \, dx_l$$

$$= \int_{F_r}\rho_r\nabla u_r(x_r) \cdot n_{F_r} \, dx_r,$$

where $J$ is the norm of the outward normal vector on the image of $\mathbf{\Phi}_{l,r}$. However, for this general case, we have the following estimate for the fluxes in the directions $-n_{F_l}$ and $n_{F_r}$.

**Proposition 2.** *Let the assumptions (2.12), (2.18) and (2.19) concerning the shape of $\Omega_g$ and the parametrization of $F_r$ hold. Then there exist positive constant $C_1 = C(\|\zeta\|_{W^{1,\infty}})$, such that*

$$\left|\int_{F_r}\rho_r\nabla u_r \cdot n_{F_r} \, dx_r - \int_{F_r}\rho_r\nabla u_r \cdot (-n_{F_l}) \, dx_r\right| \leq C_1 d_g\|\rho_r\nabla u_r\|_{L^p(F_r)}. \quad (3.17)$$

*Proof.* Let us denote $\zeta_0(x_l) = d_g\zeta(x_l)$. It follows from the form of the parametrization $\mathbf{\Phi}_{l,r}$ that $\left|n_{F_r} - (-n_{F_l})\right| = \frac{1}{J}\left|(\zeta_{0_{x_{l,1}}}, \zeta_{0_{x_{l,2}}}, 1 - J)\right|$, where $J = \sqrt{\zeta_{0_{x_{l,1}}}^2 + \zeta_{0_{x_{l,2}}}^2 + 1}$ is the norm of the outward normal vector on the image of $\mathbf{\Phi}_{l,r}$. Since $1 \leq J$, we can show that $(1 - J)^2 \leq \zeta_{x_{0_{l,1}}}^2 + \zeta_{0_{x_{l,2}}}^2$, and then it follows that

$$\left|n_{F_r} - (-n_{F_l})\right| \leq \sqrt{\zeta_{0_{x_{l,1}}}^2 + \zeta_{0_{x_{l,2}}}^2 + (1 - J)^2} \leq \sqrt{2}d_g\|\zeta\|_{W^{1,\infty}}. \quad (3.18)$$

Now, applying inequality (2.1) on the left hand side of (3.17) and using (3.18), the desired result easily follows. $\blacksquare$

**Proposition 3.** *Let the points $x_{l_0}$ on $F_l$ and the corresponding $x_{r_0} = \Phi_{l,r}(x_{l_0})$ such that $|x_{l_0} - x_{r_0}| = d_g$. Then for any $x_l \in F_l$ and $x_r = \Phi_{l,r}(x_l)$, see Fig. 3, there is a constant $C = C(|F_l|, |F_r|)$ such that*

$$\frac{|x_{l_0} - x_{r_0}|}{|x_l - x_r|} = C. \tag{3.19}$$

*Proof.* An application of Thale's theorem on the triangle $Ox_{r_0}x_{l_0}$ gives $\frac{|O-x_r|}{|O-x_{r_0}|} = \frac{|O-x_l|}{|O-x_{l_0}|}$, and $\frac{|x_{l_0}-Z|}{|x_{l_0}-x_{r_0}|} = \frac{|O-x_r|}{|O-x_{r_0}|}$. Replacing $|x_{l_0} - Z| = |x_l - x_r|$ and $|x_{l_0} - x_{r_0}| = d_g$ into the last relations, the result (3.19) follows. ∎
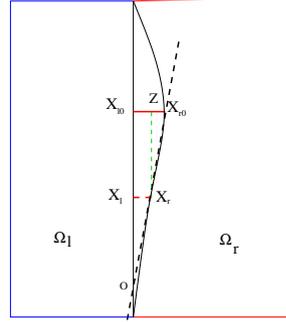


**Fig. 3.** Illustration of the ratio between the gap distance and the distance of two diametrically opposite assigned points.

## 3.2   The dG IgA problem on $\Omega \setminus \overline{\Omega}_g$

For convenience we introduce the notation $R_{\nabla,i} = \{\rho\}\left(\frac{|r_i|}{h}\nabla u_g \cdot n_{F_i} + \frac{1}{h}Ru_g(x_i)\right)$ for $i = l, r$. Recalling (3.3), the identity (3.8) and utilizing the flux approximations (3.15) and (3.16), we deduce that the exact solution $u$ satisfies

$$\int_{\Omega_l} \rho_l \nabla u \cdot \nabla \phi_h \, dx - \int_{\partial\Omega_l \cap \partial\Omega} \rho_l \nabla u \cdot n_{\partial\Omega_l} \phi_h \, d\sigma$$

$$- \int_{F_l} \left(\frac{\rho_l}{2}\nabla u_l + \frac{\rho_r}{2}\nabla u_r\right) \cdot n_{F_l}\phi_h - \frac{\{\rho\}}{h}(u_l - u_r)\phi_h \, d\sigma$$

$$+ \int_{F_l} \left\{R_{\nabla,l} + \frac{\rho_g}{2|r_l|}Ru_r(x_r) + \frac{\rho_g}{2|r_l|}Ru_g(x_l)\right\}\phi_h \, d\sigma$$

$$+ \int_{\Omega_r} \rho_r \nabla u \cdot \nabla \phi_h \, dx - \int_{\partial\Omega_r \cap \partial\Omega} \rho_r \nabla u \cdot n_{\partial\Omega_r}\phi_h \, d\sigma$$

$$- \int_{F_r} \left(\frac{\rho_r}{2}\nabla u_r + \frac{\rho_l}{2}\nabla u_l\right) \cdot n_{F_r}\phi_h - \frac{\{\rho\}}{h}(u_r - u_l)\phi_h \, d\sigma$$

$$+ \int_{F_r} \left\{R_{\nabla,r} + \frac{\rho_g}{2|r_r|}Ru_l(x_l) + \frac{\rho_g}{2|r_r|}Ru_g(x_r)\right\}\phi_h \, d\sigma$$

$$= \int_{\Omega\setminus\overline{\Omega}_g} f\phi_h \, dx, \text{ for } \phi_h \in V_h, \tag{3.20}$$

where the notation for the Taylor residuals is the same as in previous paragraph. We observe that the terms appearing in (3.20) are the terms that are expected to be appear in a dG scheme, of course, excluding the Taylor residual terms. In view of this, we define the forms $B_{\setminus\Omega_g}(\cdot,\cdot) : (V + V_h) \times V_h \to \mathbb{R}$,

$R_{\Omega_g}(\cdot,\cdot) : (V + V_h) \times V_h \to \mathbb{R}$ and the linear functional $l_{f,\backslash\Omega_g} : V_h \to \mathbb{R}$ by

$$
\begin{aligned}
B_{\backslash\Omega_g}(u,\phi_h) = &\int_{\Omega_l} \rho_l \nabla u \cdot \nabla \phi_h \, dx - \int_{\partial\Omega_l \cap \partial\Omega} \rho_l \nabla u \cdot n_{\partial\Omega_l} \phi_h \, d\sigma \\
&- \int_{F_l} \left( \frac{\rho_l}{2} \nabla u_l + \frac{\rho_r}{2} \nabla u_r \right) \cdot n_{F_l} \phi_h - \frac{\{\rho\}}{h} (u_l - u_r) \phi_h \, d\sigma \\
&+ \int_{\Omega_r} \rho_r \nabla u \cdot \nabla \phi_h \, dx - \int_{\partial\Omega_r \cap \partial\Omega} \rho_r \nabla u \cdot n_{\partial\Omega_r} \phi_h \, d\sigma \\
&- \int_{F_r} \left( \frac{\rho_r}{2} \nabla u_r + \frac{\rho_l}{2} \nabla u_l \right) \cdot n_{F_r} \phi_h - \frac{\{\rho\}}{h} (u_r - u_l) \phi_h \, d\sigma,
\end{aligned}
\tag{3.21a}
$$

$$
\begin{aligned}
R_{\Omega_g}(u,\phi_h) = &\int_{F_l} \left\{ R_{\nabla,l}\phi_h + \frac{\rho_g}{2|r_l|} R u_r(x_r)\phi_h + \frac{\rho_g}{2|r_l|} R u_g(x_l)\phi_h \right\} d\sigma \\
&+ \int_{F_r} \left\{ R_{\nabla,r}\phi_h + \frac{\rho_g}{2|r_r|} R u_l(x_l)\phi_h + \frac{\rho_g}{2|r_r|} R u_g(x_r)\phi_h \right\} d\sigma,
\end{aligned}
\tag{3.21b}
$$

$$
l_{f,\backslash\Omega_g}(\phi_h) = \int_{\Omega \backslash \overline{\Omega}_g} f\phi_h \, dx.
\tag{3.21c}
$$

We note that, the remainder integral terms $R_{\Omega_g}$ should appear in (3.20). For establishing the dG IgA discrete problem, we prefer the absence of these terms in the discrete form. Also, we wish the weak enforcement of the Dirichlet boundary conditions. Thus, for defining the dG IgA scheme, we use the forms in (3.21) and introduce the bilinear form $B_h(\cdot,\cdot) : V_h \times V_h \to \mathbb{R}$ and the linear form $F_h : V_h \to \mathbb{R}$ as follows

$$
B_h(u_h,\phi_h) = B_{\backslash\Omega_g}(u_h,\phi_h) + \sum_{i=l,r} \frac{\rho_i}{h} \int_{\partial\Omega_i \cap \partial\Omega} u_h \phi_h \, d\sigma,
\tag{3.22}
$$

$$
F_h(\phi_h) = l_{f,\backslash\Omega_g}(\phi_h) + \sum_{i=l,r} \frac{\rho_i}{h} \int_{\partial\Omega_i \cap \partial\Omega} u_D \phi_h \, d\sigma.
\tag{3.23}
$$

We consider the discrete problem: find $u_h \in V_h$ such that

$$
B_h(u_h,\phi_h) = F_h(\phi_h), \quad \text{for all } \phi_h \in V_h.
\tag{3.24}
$$

An immediate result is that, for the exact solution $u \in V$, the variational identity

$$
B(u,\phi_h) := B_h(u,\phi_h) + R_{\Omega_g}(u,\phi_h) = F_h(\phi_h), \ \forall \phi \in V_h,
\tag{3.25}
$$

holds. Next we show several results that are going to be used in the error analysis.

**Lemma 1.** *Let $\frac{1}{q} = \frac{p-1}{p}$ and $\gamma_{p,d} = \frac{1}{2}d(p-2)$. Then there exist a constant $C \geq 0$ independent of $h$ such that the estimate*

$$
\frac{1}{h^{\frac{1+\gamma_{p,d}}{p}}} \|\phi_h\|_{L^q(F_i)} \leq Ch^{-\frac{1}{2}} \|\phi_h\|_{L^2(F_i)}, \ \text{for } i = l,r,
\tag{3.26}
$$

*holds for every $\phi_h \in V_h$.*

*Proof.* The lemma is proven in [16]. ∎

**Lemma 2.** *Let $\gamma_{p,d} = \frac{1}{2}d(p-2)$. Then there is a constant $C \geq 0$ independent of $h$ such that the estimate*

$$
B_h(u,\phi_h) \leq C \Big( \|u\|_{dG}^p + \sum_{i=l,r} h^{1+\gamma_{p,d}} \|\nabla u_i\|_{L^p(\partial\Omega_i)}^p \Big)^{\frac{1}{p}} \|\phi_h\|_{dG},
\tag{3.27}
$$

*holds for all $(u,\phi_h) \in (V + V_h) \times V_h$.*

*Proof.* We first give a bound for the normal flux terms on $\partial\Omega_l$. A direct application of Lemma 5.2 in [16] gives

$$\int_{\partial\Omega_l\cap\partial\Omega} \rho_l\nabla u \cdot n_{\partial\Omega_l}\phi_h\,d\sigma \leq C\Big(h^{1+\gamma_{p,d}}\|\nabla u_l\|_{L^p(\partial\Omega_l\cap\partial\Omega)}^p\Big)^{\frac{1}{p}}\|\phi_h\|_{dG}. \tag{3.28}$$

Let $J$ be the norm of the outward normal vector on the image of $\mathbf{\Phi}_{l,r}$. For the flux terms on $F_l$, the triangle and (2.1) inequalities yield

$$\int_{F_l}\Big(\frac{\rho_l}{2}\nabla u_l + \frac{\rho_r}{2}\nabla u_r\Big)\cdot n_{F_l}\phi_h\,d\sigma \leq \Big|\int_{F_l}(\rho_l h^{1+\gamma_{p,d}})^{\frac{1}{p}}\nabla u_l \cdot n_{F_l}\frac{\rho_l^{\frac{1}{q}}}{h^{\frac{1+\gamma_{p,d}}{p}}}\phi_h\,d\sigma\Big|$$

$$+\Big|\int_{F_l}(\rho_r h^{1+\gamma_{p,d}})^{\frac{1}{p}}\nabla u_r \cdot n_{F_l}J^{-1}J\frac{\rho_r^{\frac{1}{q}}}{h^{\frac{1+\gamma_{p,d}}{p}}}\phi_h\,d\sigma\Big|$$

$$\leq C_1(\rho_l)h^{\frac{1+\gamma_{p,d}}{p}}\|\nabla u_l\|_{L^p(F_l)}\frac{1}{h^{\frac{1+\gamma_{p,d}}{p}}}\|\phi_h\|_{L^q(F_l)} + C_2(\rho,J^{-1})h^{\frac{1+\gamma_{p,d}}{p}}\|\nabla u_r\|_{L^p(F_r)}\frac{1}{h^{\frac{1+\gamma_{p,d}}{p}}}\|\phi_h\|_{L^q(F_l)}$$

$$\leq C_3(\rho,J^{-1})h^{\frac{1+\gamma_{p,d}}{p}}\Big(\|\nabla u_l\|_{L^p(F_l)} + \|\nabla u_r\|_{L^p(F_r)}\Big)\|\phi_h\|_{dG}, \tag{3.29}$$

where the estimate (3.26) and relations (2.21) have been used. The flux terms of $B_h(\cdot,\cdot)$, which appear on $F_r$ can be bound in a similar way. As a last step, we need to bound the jump terms in $B_h(\cdot,\cdot)$. Following similar procedure as in (3.29), we can show

$$\sum_{i=l,r}\int_{\Omega_i}\rho_i\nabla u\cdot\nabla\phi_h\,dx + \int_{F_i}\frac{\{\rho\}}{h}(u_i - u_j)\phi_h\,d\sigma \leq C\|u\|_{dG}\|\phi_h\|_{dG}, \text{ for } j=r,l \text{ and } j\neq i. \tag{3.30}$$

Finally, collecting all the above bounds we can deduce assertion (3.27).  ∎

Now, we prove that the discrete problem (3.24) has unique solution.

**Lemma 3.** *The bilinear form $B_h(\cdot,\cdot)$ in (3.22) is bounded and elliptic on $V_h$, i.e., there are positive constants $C_M$ and $C_m$ such that the estimates*

$$B_h(v_h,\phi_h) \leq C_M\|v_h\|_{dG}\|\phi_h\|_{dG} \quad and \quad B_h(v_h,v_h) \geq C_m\|v_h\|_{dG}^2, \tag{3.31}$$

*hold for all $\phi_h \in V_h$.*

*Proof.* The two properties of $B_h(\cdot,\cdot)$ can be shown following the same procedure as in Lemma 2 and mimic the proofs of Lemma 4.5 and Lemma 4.6 in [16]. Thus, the details are omitted.  ∎

Since $B_h(.,.)$ is bounded and elliptic in $V_h$, we can apply the Lax-Milgram theorem to conclude that the problem (3.24) has a unique solution.

One of the most important properties of the dG discretization is its consistency. This ensures that the "right" equations are solved. Consistency yields Galerkin orthogonality. Here, the solution $u$ satisfies (3.25) but does not satisfy the discrete problem (3.24). We derive the error analysis borrowing ideas from the weak consistent FE methods, [9]. We start with the derivation of uniform bounds for the $R_{\Omega_g}(u,\phi_h)$ terms.

## 3.3   Estimates of the remainder terms

We proceed by deriving estimates for general order Taylor remainder terms, see (3.12). We have the following estimate.

**Lemma 4.** *For $(u,\phi_h) \in V \times V_h$, and for $i=l,r$ there is a positive constant $C$, such that*

$$\frac{|r_i|}{h}\Big|\int_{F_i}\rho_g\nabla u_g\cdot n_{F_i}\phi_h\,d\sigma\Big| \leq Ch^{\lambda-1}h^{\frac{1+\gamma_{p,d}}{p}}\|\nabla u_g\|_{L^p(F_i)}\|\phi_h\|_{dG}, \tag{3.32}$$

*where $\gamma_{p,d} = \frac{1}{2}d(p-2)$.*

*Proof.* Following the same arguments as in estimate (3.29), we can show that

$$\Big| \int_{F_i} \rho_g \nabla u_g \cdot n_{F_i} \phi_h \, d\sigma \Big| \le C h^{\frac{1+\gamma_{p,d}}{p}} \|\nabla u_g\|_{L^p(F_i)} \|\phi_h\|_{dG}. \tag{3.33}$$

Observing that $\frac{|r_i|}{h} \sim \frac{d_g}{h} \le h^{\lambda-1}$, see (2.18), the desired bound follows. ∎

**Lemma 5.** *Let Assumption 4 hold. Then there exist a positive constant $C = C(l, p, d)$ such that for all $(u, \phi_h) \in V \times V_h$ holds*

$$s_{F_l}(u, \phi_h) = \frac{1}{h} \int_{F_l} \phi_h(x_l) \int_0^1 \sum_{|\alpha|=l} (x_r - x_l)^\alpha \frac{l}{\alpha!} s^{l-1} D^\alpha u(x_r + s(x_l - x_r)) \, ds \, dx_l \le$$

$$C \, d_g^l \, h^\zeta \, d_g^{-\frac{p(l-d-1)+1}{p}} \|\phi_h\|_{dG} \Big( \int_{\Omega_g} \kappa_l(z)^p \, dz \Big)^{\frac{1}{p}}, \quad (3.34)$$

*where $l \ge 2$, $\zeta = \frac{-2(p-1)+d(p-2)}{2p}$ and $\kappa_l(z) = \big( \sum_{|\alpha|=l} |D^\alpha u(z)| \big)$.*

*Proof.* We set $\frac{1}{q} = \frac{p-1}{p}$ and $\gamma = \frac{2+d(p-2)}{2p}$. We fix an edge $e_l \subset F_l$ such that $e_l \subset \partial E_l$, where the micro-element $E_l \in T_{h,\Omega_l}^{(l)}$ touches $F_l$. We note that Assumption 2 gives $|e_l| \sim h^{d-1}$. Inequality (2.1) yields

$$s_{e_l}(u, \phi_h) = \frac{1}{h^{\frac{1}{p}+\frac{1}{q}+\frac{d(p-2)}{2p}}} \int_{e_l} \phi_h(x_l) \int_0^1 h^{\frac{d(p-2)}{2p}} \sum_{|\alpha|=l} (x_r - x_l)^\alpha \frac{l}{\alpha!} s^{l-1} D^\alpha u(x_r + s(x_l - x_r)) \, ds \, dx_l$$

$$= \int_{e_l} \int_0^1 \frac{1}{h^\gamma} \phi_h(x_l) \sum_{|\alpha|=l} h^{\frac{-2(p-1)+d(p-2)}{2p}} (x_r - x_l)^\alpha \frac{l}{\alpha!} s^{l-1} D^\alpha u(x_r + s(x_l - x_r)) \, ds \, dx_l$$

$$\le C \frac{1}{h^\gamma} \Big( \int_{e_l} \int_0^1 |\phi_h|^q \, ds \, dx_l \Big)^{\frac{1}{q}} h^\zeta \, d_g^l \Big( \int_{e_l} \int_0^1 \big( \sum_{|\alpha|=l} s^{l-1} |D^\alpha u(x_r + s(x_l - x_r))| \big)^p \, ds \, dx_l \Big)^{\frac{1}{p}}. \tag{3.35}$$

Using the discrete inequalities (3.26), we obtain that

$$\frac{1}{h^\gamma} \Big( \int_{e_l} \int_0^1 |\phi_h|^q \, ds \, dx_l \Big)^{\frac{1}{q}} \le C_{p,d} \Big( \frac{1}{h} \int_{e_l} \phi_h^2 \, dx_l \Big)^{\frac{1}{2}} = C_{p,d} h^{\frac{-1}{2}} \|\phi_h\|_{L^2(e_l)}. \tag{3.36}$$

It remains to estimate the second term in (3.35) on every $e_l$. By the change of variables $z = x_r + s(x_l - x_r)$, we have that

$$(x_r - z)s^{-1} = (x_r - x_l), \tag{3.37a}$$

$$\big( x_{l_1}, x_{l_2}, ..., x_{l_d} \big) = \big( x_{r_1}(x_l), x_{r_2}(x_l), ..., x_{r_d}(x_l) \big) + \tag{3.37b}$$

$$s^{-1} \big( z_1, z_2, ..., z_d \big) - \big( x_{r_1}(x_l), x_{r_2}(x_l), ..., x_{r_d}(x_l) \big)$$

$$(z - x_r)^\alpha s^{-l} = (x_r - x_l)^\alpha, \tag{3.37c}$$

$$\det \Big( \frac{\partial(x_l, s)}{\partial(z, s)} \Big) = s^{-d}. \tag{3.37d}$$

*Remark 5.* The previous relations have been given for a general gap region. For the gaps described in Subsection 2.4, see Fig. 2, the relations (3.37) take the form

$$x_{r_1}(x_l) := x_{r_1} = x_{l_1}$$
$$x_{r_2}(x_l) := x_{r_2} = x_{l_2}$$
$$x_{r_3}(x_l) := x_{r_3}(x_{l_1}, x_{l_2}) = d_g \, \zeta(x_l),$$

and it can be verified that $\det \Big( \frac{\partial(x_l, s)}{\partial(z, s)} \Big) = s^{-1}$.

Now, let $z$ be any point in the interval $(x_l, x_r)$. Moreover, let $x_{l_0}$ and $x_{r_0} = \Phi_{l,r}(x_{l_0})$ be as in Proposition 3. Then we can deduce that

$$|z - x_r| \leq |z - x_{r_0}| + |x_r - x_{r_0}|, \quad |x_r - x_l| = C d_g. \tag{3.38}$$

Now, since the parameter $s$ varies between 0 and 1, the variable $z$ also runs in the region $E_g \subset \Omega_g$ with $|E_g| \leq d_g h^{d-1}$, see Fig. 2(c). Describing the domain with respect to $(z, s)$ variables, the range of $s$ is defined to be such that the $\omega(z, s) := (z - x_r)\frac{1}{s} + x_r$, should remain in $e_l$. Using (3.37), (3.38) and the fact that that $diameter(e_l) \sim h$ the new variables satisfy

$$\left| (z - x_r)\frac{1}{s} + x_r \right| \leq C_\theta h, \text{ and } s \leq \frac{|z - x_{r_0}| + |x_r - x_{r_0}|}{C d_g} = \frac{C_{\Omega_g}}{d_g}, \tag{3.39}$$

where the constant $C_\theta > 0$ depends on the quasi-uniformity properties of the meshes, see Assumption 2, and $C_{\Omega_g} > 0$ on the shape of $\Omega_g$. Thus, by the change of the order of integration and by the change of variable on the second term in (3.35), we get

$$\left( \int_{e_l} \int_0^1 \Big( \sum_{|\alpha|=l} s^{l-1} |D^\alpha u(x_r + s(x_l - x_r))| \Big)^p ds \, dx_l \right)^{\frac{1}{p}} = \left( \int_0^1 \int_{\omega(z,s)=x_l} \Big( s^{l-d-1} \sum_{|\alpha|=l} |D^\alpha u(z)| \Big)^p dz \, ds \right)^{\frac{1}{p}}$$

$$\leq C \left( \int_{E_g} \int_0^{\frac{C_{\Omega_g}}{d_g}} \Big( s^{l-d-1} \sum_{|\alpha|=l} |D^\alpha u(z)| \Big)^p ds \, dz \right)^{\frac{1}{p}} \leq C \left( \int_{E_g} s^{p(l-d-1)+1} \Big|_0^{\frac{C_{\Omega_g}}{d_g}} \Big( \sum_{|\alpha|=l} |D^\alpha u(z)| \Big)^p dz \right)^{\frac{1}{p}}$$

$$\leq C \left( \int_{E_g} \Big( \frac{C_{\Omega_g}}{d_g} \Big)^{p(l-d-1)+1} \kappa_l(z)^p \, dz \right)^{\frac{1}{p}} \leq C d_g^{-\frac{(p(l-d-1)+1)}{p}} \left( \int_{E_g} \kappa_l(z)^p \, dz \right)^{\frac{1}{p}}. \tag{3.40}$$

Finally, inserting (3.36) and (3.40) into (3.35), and then summing over all $e_l \subset F_l$, we obtain

$$s_{F_l}(u, \phi_h) \leq C \Big( \sum_{e_l \subset F_l} \Big( \frac{1}{h^{\frac{1}{2}}} \|\phi_h\|_{L^2(e_l)} \Big)^q \Big)^{\frac{1}{q}} d_g^l h^\zeta d_g^{-\frac{(p(l-d-1)+1)}{p}} \Big( \sum_{E_g \subset \Omega_g} \int_{E_g} \kappa_l(z)^p \, dz \Big)^{\frac{1}{p}}. \tag{3.41}$$

Using the fact that the $f(x) = (\eta_0 \alpha^x + \eta_0 \beta^x)^{\frac{1}{x}}$, $\eta_0 > 0, x > 2$ is decreasing, we have the inequality

$$\Big( \sum_{e_l \subset F_l} \Big( \frac{1}{h^{\frac{1}{2}}} \|\phi_h^2\|_{L^2(e_l)} \Big)^q \Big)^{\frac{1}{q}} \leq C \Big( \frac{1}{h} \|\phi_h\|_{L^2(F_l)}^2 \Big)^{\frac{1}{2}} \leq C \|\phi_h\|_{dG}. \tag{3.42}$$

We insert (3.42) into (3.41), and then we deduce (3.34). ∎

Working in a similar way as in the proof of Lemma 5, we can show similar bounds for the other remainder terms, i.e.,

$$s_{F_r}(u, \phi_h) = \frac{1}{h} \int_{F_r} \phi_h(x_r) \int_0^1 \sum_{|\alpha|=l} (x_l - x_r)^\alpha \frac{l}{\alpha!} s D^\alpha u(x_l + s(x_r - x_l)) \, ds \, dx_r$$

$$\leq C \|\phi_h\|_{dG} d_g^l h^\zeta d_g^{-\frac{(p(l-d-1)+1)}{p}} \Big( \int_{\Omega_g} \kappa_l(z)^p \, dz \Big)^{\frac{1}{p}}. \tag{3.43}$$

We continue to give an estimate for the $R_{\Omega_g}(\cdot, \cdot)$ defined in (3.21).

**Lemma 6.** *Under the Assumptions 2 and 4, there exist a positive constant $C = C(\rho, p, d, l)$, such that the estimate*

$$|R_{\Omega_g}(u, \phi_h)| \leq C \|\phi_h\|_{dG} \big( \|\nabla u_g\|_{L^p(\partial \Omega_g)} + \|\kappa_2\|_{L^p(\Omega_g)} \big) h^\beta, \tag{3.44}$$

*holds true for all $(u, \phi_h) \in V \times V_h$, where $\kappa_2 = \big( \sum_{|\alpha|=2} |D^\alpha u| \big)$, $\zeta = \frac{-2(p-1)+d(p-2)}{2p}$, and $\beta = \min\{2\lambda + \zeta - \frac{p(1-d)+1}{p}, \lambda - 1 + \frac{1+\gamma_{p,d}}{p}, 1 + \zeta + \lambda - \frac{p(1-d)+1}{p}\}$,*

*Proof.* Clearly, Proposition 3 in combination with Assumption 2 imply that $|r_l| \sim h^\lambda$ and $|r_r| \sim h^\lambda$. Recalling the definition of $R_{\Omega_g}(\cdot, \cdot)$, see (3.21), and using the estimates (3.32), (3.34) and (3.43) with $|\alpha| = 2$, we can derive

$$
|R_{\Omega_g}(u, \phi_h)| \le C \Big( h^{\lambda-1} h^{\frac{1+\gamma_{p,d}}{p}} \|\nabla u_g\|_{L^p(\partial\Omega_g)}
$$
$$
+ d_g^2 \, h^\zeta \, d_g^{-\frac{p(2-d-1)+1}{p}} \|\kappa_2\|_{L^p(\Omega_g)}
$$
$$
+ d_g^2 \, h^{\zeta+1-\lambda} d_g^{-\frac{p(2-d-1)+1}{p}} \|\kappa_2\|_{L^p(\Omega_g)} \Big) \|\phi_h\|_{dG}, \quad (3.45)
$$

where the constant depends on the constant in (3.32), the constant in (3.34) and the quasi-uniformity parameters of the mesh, see Assumption 2. Setting $d_g \sim h^\lambda$ in (3.45), we immediately arrive at estimate (3.44). ∎

## 4    Error estimates

Next, we give an error estimate by means of a variation of Cea's Lemma applied in dG frame. We use the estimate for $|R_{\Omega_g}(u, \phi_h)|$ as is given in (3.44). The linearity of the $B_h(\cdot, \cdot)$, see (3.22) and (3.21), and the discrete variational form (3.24) yield

$$
B_h(u_h - z_h, \phi_h) = F_h(\phi_h) - B_h(z_h, \phi_h), \quad \text{for all} \quad \phi_h, \, z_h \in V_h. \quad (4.1)
$$

Using (3.21), (3.22), (3.23) and (3.25), we get

$$
B_h(u_h - z_h, \phi_h) = B(u, \phi_h) + \sum_{i=l,r} \frac{\rho_i}{h} \int_{\partial\Omega_i \cap \partial\Omega} (u - u_D)\phi_h \, d\sigma - B_h(z_h, \phi_h) + F_h(\phi_h) - l_{f, \backslash \overline{\Omega}_g}(\phi_h)
$$
$$
= B_h(u, \phi_h) + R_{\Omega_g}(u, \phi_h) - \sum_{i=l,r} \frac{\rho_i}{h} \int_{\partial\Omega_i \cap \partial\Omega} u_D \phi_h \, d\sigma - B_h(z_h, \phi_h) + \sum_{i=l,r} \frac{\rho_i}{h} \int_{\partial\Omega_i \cap \partial\Omega} u_D \phi_h \, d\sigma
$$
$$
= B_h(u - z_h, \phi_h) + R_{\Omega_g}(u, \phi_h). \quad (4.2)
$$

We choose in (4.2) $\phi_h = u_h - z_h$. Then, Lemma 3 and Lemma 2 imply

$$
C_m \|u_h - z_h\|_{dG}^2 \le C_M \big( \|u - z_h\|_{dG}^p + h^{1+\gamma_{p,d}} \|\nabla(u - z_h)\|_{L^p(\partial\Omega_g)}^p \big)^{\frac{1}{p}} \|u_h - z_h\|_{dG} + |R_{\Omega_g}(u, u_h - z_h)|
$$
$$
\le C_M \big( \|u - z_h\|_{dG}^p + h^{1+\gamma_{p,d}} \|\nabla(u - z_h)\|_{L^p(\partial\Omega_g)}^p \big)^{\frac{1}{p}} \|u_h - z_h\|_{dG} + C_1 \|u_h - z_h\|_{dG} h^\beta \mathcal{K}_p, \quad (4.3)
$$

where we previously used the estimate (3.44) and $\mathcal{K}_p = \|\nabla u_g\|_{L^p(\partial\Omega_g)} + \|\kappa_2\|_{L^p(\Omega_g)}$. Applying triangle inequality in (4.3), we can easily arrive at the following estimate

$$
\|u - u_h\|_{dG} \le C \Big( \big( \|u - z_h\|_{dG}^p + h^{1+\gamma_{p,d}} \|\nabla(u - z_h)\|_{L^p(\partial\Omega_g)}^p \big)^{\frac{1}{p}} + h^\beta \mathcal{K}_p \Big), \quad (4.4)
$$

where the constant $C$ is specified by the constants appearing in (4.3).

Now, we can prove the main error estimate result of the section. Such an estimate requires quasi-interpolation estimates of B-splines. By the results of multidimensional B-spline interpolation, (see [24] and [16]), we can construct a quasi-interpolant $\Pi : W^{l,p} \to V_h$ with $l \ge 1, p > 1$, such that the following interpolation estimates to be true.

**Lemma 7.** *Let* $u \in W^{l,p}(\Omega_i)$ *with* $l \ge 2$, $p \in (\max\{1, \frac{2d}{d+2(l-1)}\}, 2]$. *Then for* $i = l, r$, *there exist constants* $C_i$ *such that*

$$
h^{\frac{1+\gamma_{p,d}}{p}} \|\nabla(u - \Pi u)\|_{L^p(\partial\Omega_i)} \le C_i h^{\delta_\Pi(l,p,d)} \|u\|_{W^{l,p}(\Omega_i)}, \quad (4.5a)
$$
$$
\frac{\{\rho_i\}}{h} \big( \|u - \Pi u\|_{L^2(\partial\Omega_i)} \big)^2 \le C_i \big( h^{\delta_\Pi(l,p,d)} \|u\|_{W^{l,p}(\Omega_i)} \big)^2, \quad (4.5b)
$$

*where* $\delta_\Pi(l,p,d) = l + (\frac{d}{2} - \frac{d}{p} - 1)$ *and* $\gamma_{p,d} = \frac{1}{2}d(p-2)$.

*Proof.* The proofs are given in [16] for the general case of non-matching grids. ∎

**Lemma 8.** *Let $u$ satisfy Assumption 1. Then, there exist constants $C_i > 0$ with $i = l, r$ independent of the grid sizes $h$ such that*

$$\|u - \Pi u\|_{dG} \leq \sum_{i=l,r} C_i h^{\delta_\Pi(l,p,d)} \|u\|_{W^{l,p}(\Omega_i)}, \tag{4.6}$$

*where $\delta_\Pi(l,p,d) = l + (\frac{d}{2} - \frac{d}{p} - 1)$.*

*Proof.* We show first an estimate for $E \in T^{(i)}_{h,\Omega_i}$ for $i = l, r$. We associate with each $E \in T^{(i)}_{h,\Omega_i}$ the local support extension $D^{(i)}_E$ of the B-splines, see Subsection 2.3. By the properties of the quasi-interpolant $\Pi$ we have the estimate, see [16],

$$|u - \Pi u|_{W^{1,p}(E)} \leq C h^{l-1} \|u\|_{W^{l,p}(D^{(i)}_E)}. \tag{4.7}$$

We quote below an inequality which holds for $f$ satisfying Assumption 1 and has been shown in [16],

$$\|f\|_{L^2(E)} \leq C_i h^{\frac{d}{2} - \frac{d}{p}} \left( \|f\|^p_{L^p(E)} + h^p |f|^p_{W^{1,p}(E)} \right)^{\frac{1}{p}}, \text{ for } E \in T^{(i)}_{h,\Omega_i}, \ i = l, r. \tag{4.8}$$

Setting $f := \nabla u - \nabla \Pi u$ in (4.8), summing over all micro-elements and applying the approximation estimate (4.7), we obtain that

$$|u - \Pi u|^2_{W^{1,2}(\Omega_i)} \leq C_i \left( h^{l+(\frac{d}{2} - \frac{d}{p} - 1)} \|u\|_{W^{l,p}(\Omega_i)} \right)^2, \text{ for } i = l, r. \tag{4.9}$$

It remains to estimate the jump terms in dG-norm. We apply (4.5b) and get

$$\sum_{i=l,r} \frac{\{\rho\}}{h} \int_{F_i} |u_i - \Pi u_i|^2 \, d\sigma \leq \sum_{i=l,r} C_i \left( h^{\delta_\Pi(l,p,d)} \|u\|_{W^{l,p}(\Omega_i)} \right)^2, \tag{4.10}$$

Recalling the definition of $\|.\|_{dG}$, combining the estimates (4.9) and (4.10) we can derive (4.6). ∎

**Theorem 1.** *Let $u$ be the solution of problem (3.25), $u_h$ be the corresponding dG IgA solution of problem (3.24), and let $d_g = h^\lambda$ with $\lambda \geq 1$. Then the error estimate*

$$\|u - u_h\|_{dG} \lesssim h^{\delta_\Pi(l,p,d)} \sum_{i=l,r} \|u\|_{W^{2,p}(\Omega_i)} + h^\beta \mathcal{K}_p, \tag{4.11}$$

*holds, where $\delta_\Pi(l,p,d) = l + (\frac{d}{2} - \frac{d}{p} - 1)$, $\mathcal{K}_p = \|\nabla u_g\|_{L^p(\partial \Omega_g)} + \|\kappa_2\|_{L^p(\Omega)}$,
$\kappa_2 = \left( \sum_{|\alpha|=2} |D^\alpha u| \right)$, $\beta = \min\{2\lambda + \zeta - \frac{p(1-d)+1}{p}, \lambda - 1 + \frac{1+\gamma_{p,d}}{p}, 1 + \zeta + \lambda - \frac{p(1-d)+1}{p}\}$,
$\zeta = \frac{-2(p-1)+d(p-2)}{2p}$, $\gamma_{p,d} = \frac{1}{2}d(p-2)$ and the positive constants $C_i$ are the same as in (4.6)*

*Proof.* The required estimate follows easily by introducing the quasi-interpolation estimates (4.5a) and (4.6) into estimate (4.4). ∎

## 5   Numerical tests

We have performed a few numerical tests in order to confirm the theoretically predicted order of accuracy for the dG IgA scheme proposed in (3.22). We will discuss two- and three- dimensional test examples.

All tests have been performed using second order ($k = 2$) B-spline spaces. Every example has been solved applying several mesh refinement steps with $h_i, h_{i+1}, ...$, satisfying Assumption 2. The numerical convergence rates $r$ have been computed by the ratio $r = ln(e_i/e_{i+1})/ln(h_i/h_{i+1})$, $i = 1, 2, ...$, where the error $e_i := \|u - u_h\|_{dG}$ is always computed on the meshes $T^{(l)}_{h_i,\Omega_l} \cup T^{(r)}_{h_i,\Omega_r}$. We mention that, in the test cases with highly smooth solutions, i.e., $k+1 \le l$, the approximation order in (4.11) becomes $\delta_\Pi(l, p, d) = k$.

The code that has been materialized for performing the tests uses unidirectional Taylor expansions, see (2.15), Remark 4 and Remark 5. The predicted values of power $\beta$ in (4.11) are given in Table 2.

For the two dimensional examples, we use the knot vectors $\Xi^1_i = \Xi^2_i := \{0, 0, 0, 0.5, 0.5, 1, 1, 1\}$, with $i = l, r$, to define the parametric mesh and to construct the coresponding second order B-spline space, see (2.6). The B-spline parametrizations of $\Omega_l$ and $\Omega_r$, see (2.8), are constructed using the control points which are listed in Table 1. In any test case, the gap region is artificially created by moving all control points of the second subdomain which have the form $(0, \xi)$, where $0 < \xi < 1$, in the direction $(1, 0)$, For all tests, the parametric mapping in (2.19) has the form $\boldsymbol{\Phi}_{l,r}(x_1, x_2) = (x_1, x_2) + d_g 4x_2(1 - x_2)(1, 0)$.

| | $\boldsymbol{\Phi}_l$ | $\boldsymbol{\Phi}_r$ |
|---|---|---|
| | (-1, -0.2) | (0, 0) |
| | (-0.75, 0) | (0.25, 0) |
| | (-0.5, 0) | (0.5, 0) |
| | (-0.25, 0) | (0.75, 0) |
| | (0, 0) | (1, 0.2) |
| | (-1, 0.25) | (0, 0.25) |
| | (-0.75, 0.25) | (0.25, 0.25) |
| | (-0.5, 0.25) | (0.5, 0.25) |
| | (-0.25, 0.25) | (0.75, 0.25) |
| | (0, 0.25) | (1, 0.25) |
| | (-1, 0.5) | (0, 0.5) |
| | (-0.75, 0.5) | (0.25, 0.5) |
| | (-0.5, 0.5) | (0.5, 0.5) |
| | (-0.25, 0.5) | (0.75, 0.5) |
| | (0, 0.5) | (1, 0.5) |
| | (-1, 0.75) | (0, 0.75) |
| | (-0.75, 0.75) | (0.25, 0.75) |
| | (-0.5, 0.75) | (0.5, 0.75) |
| | (-0.25, 0.75) | (0.75, 0.75) |
| | (0, 0.75) | (1, 0.75) |
| | (-1, 1.2) | (0,1) |
| | (-0.75, 1) | (0.25,1) |
| | (-0.5, 1) | (0.5, 1) |
| | (-0.25, 1) | (0.75, 1) |
| | (0, 1) | (1, 0.8) |

**Table 1.** The control points for the mappings $\boldsymbol{\Phi}_i$, $i = l, r$.

| | B-spline degree $k = 2$ | | |
|---|---|---|---|
| | Smooth solutions, $u \in W^{l>3,p=2}$ | | |
| $d_g = h^\lambda$ | $\lambda = 1$ | $\lambda = 2$ | $\lambda = 3$ |
| $\beta :=$ | 0.5 | 1.5 | 2 |
| $\delta_\Pi(l, p, d) :=$ | 2 | 2 | 2 |

**Table 2.** The values of the order $\beta$ of the remainder term bounds and the B-spline approximation order.

| - | $d_g = h^\lambda$ | | |
|---|---|---|---|
| - | $\lambda = 1$ | $\lambda = 2$ | $\lambda = 3$ |
| - | expected rates $r$ | | |
| $\gamma = 0.42$, $u \in W^{2,1.26}$ | 0.22 | 0.42 | 0.42 |
| $\gamma = 0.38$, $u \in W^{2,1.23}$ | 0.19 | 0.38 | 0.38 |
| $\gamma = 1$, $u \in W^{2,2}$ | 0.5 | 1 | 1 |
| $\gamma = 1.5$, $u \in W^{2.5,2}$ | 0.5 | 1.5 | 1.5 |
| $\gamma = 2$, $u \in W^{3,2}$ | 0.5 | 1.5 | 2 |

**Table 3.** The expected values of the rates $r$ for the example with low regularity solution.

## 5.1 Two-dimensional numerical examples

*Example 1.* The domain $\Omega$ with the subdomains $\Omega_l$, $\Omega_r$ and $\Omega_g$ are shown in Fig. 4(a). The Dirichlet boundary condition and the right hand side $f$ are determined by the exact solution $u(x_1, x_2) = \sin(5\pi x_1)\sin(4\pi x_2)$. In this example, we consider the homogeneous diffusion case, i.e., $\rho_l = \rho_r = 1$, and the left interface is given by $F_l = \{(x_{l,1}, x_{l,2}) : x_{l_1} = 0, 0 \le x_{l,2} \le 1\}$, see Fig. 4(a). We performed two computations. In the first computation, the size of $d_g$ was successively defined to be $\mathcal{O}(h^\lambda)$, with $\lambda = 1, 2$ and 3. The numerical convergence rates for several levels of mesh refinement are plotted in Fig. 4(b). They are in good agreement with our theoretically predicted estimates given in Theorem 1, see also Table 2. In the second computation, we progressively decrease the size of $d_g$ when we are performing the computation on successively refined meshes. In Fig. 4(c), we present the corresponding convergence rates $r$. For the first meshes, we set $d_g = h$, and the rates are $r = 0.5$, for the next, we set $d_g = h^2$ and the rates are increased to $r = 1.5$, behaving according to the rates predicted by the theory. Finally, for the last refinement levels, we set $d_g = h^3$, and the rates become optimal having similar behavior as in Fig. 4(b).

*Example 2.* We consider the problem with discontinuous coefficient, i.e., we set $\rho_1 = 4\pi$ in $\Omega_1$ and $\rho_2 = 1$ in $\Omega_2$. The domain $\Omega$ is presented in Fig. 4(a), where the interface $F$ is the $x_2$-axis. The solution is given by the formula

$$u(x_1, x_2) = \begin{cases} \exp(x_1) - 1 & \text{if } (x_1, x_2) \in \Omega_1, \\ \sin(4\pi x_1) & \text{if } (x_1, x_2) \in \Omega_2. \end{cases} \tag{5.1}$$
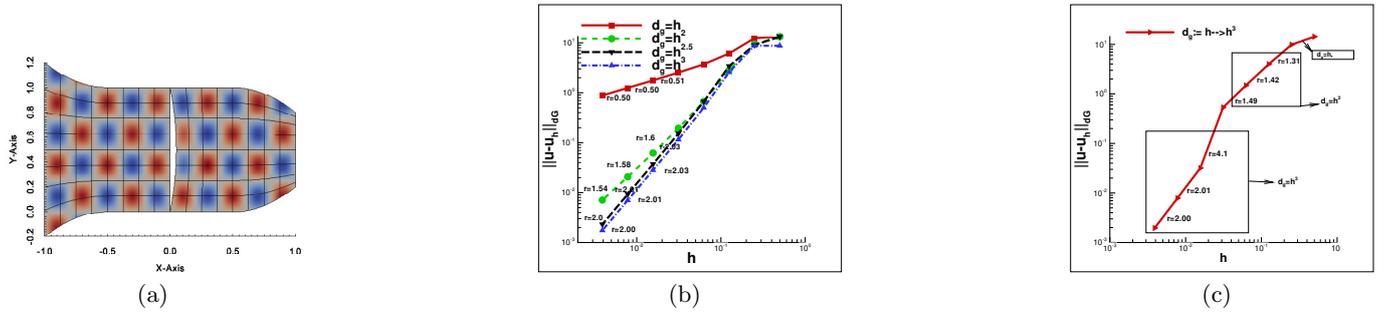
**Fig. 4.** Example 1: (a) The subdomains $\Omega_l$, $\Omega_r$ and $\Omega_g$ and the exact solution contours, (b) The convergence rates for $d_g = \mathcal{O}(h^\lambda)$, (c) The convergence rates for fixed $d_g$.

The boundary conditions and the source function $f$ are determined by (5.1). Note that in this test case, we have $[\![u]\!]|_F = 0$ as well $[\![\rho\nabla u]\!]|_F = 0$ for the normal flux on $F$. The contours of the exact solution on the domain $\Omega$ are presented in Fig. 5(a). The problem has been solved on meshes refined following a sequential process, where we set $d_g = h^\lambda$, with $\lambda = 1, 2$ and 3. Thus for every computation the gap boundary is formed by the choice of $h$ and $\lambda$. In Fig. 5(b), we plot the $u_h$ solution on $\Omega \setminus \Omega_g$ computed on a grid with $h = 0.125$ and $d_g = 0.1$. The computed rates are presented in Fig. 5(c). For the cases where $\lambda = 1$ and $\lambda = 2$, we observe that the values of the rates behave according to the predicted rates, see (4.11). The error corresponding to the $d_g = h^3$ test case (dashed dot line) on the first refinements appears to decay slower than it was expected, but finally on the last refinement levels tends to take the optimal value, which has predicted by the theory. By this example we validate numerically the predicted convergence rates for problems with discontinuous coefficient and smooth solutions.
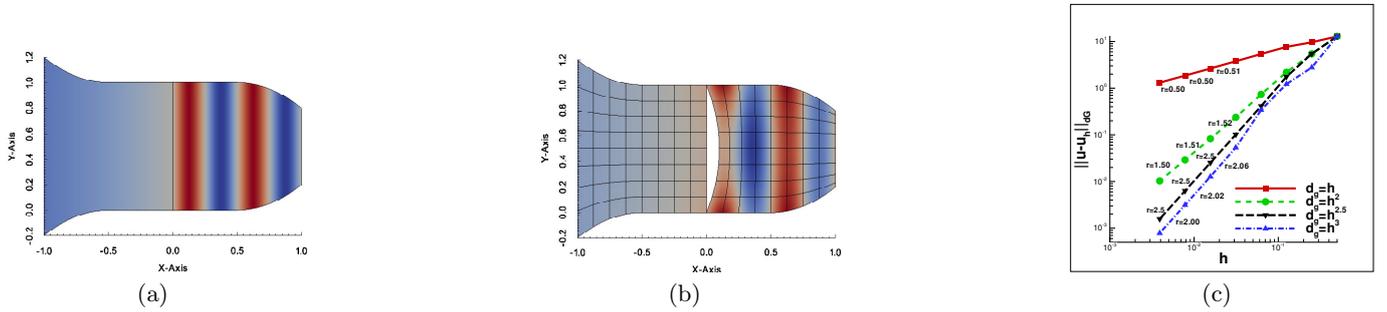


**Fig. 5.** Example 2: (a) The contours of exact $u$ given by (5.1), (b) The contours of $u_h$ on subdomains $\Omega_l$, $\Omega_r$ , (c) The convergence rates for the three choices of $\lambda$.

*Example 3.* This example consists of problem with low regularity solution, i.e., $u(x_1, x_2) = ((x_1 - 0)^2 + (x_2 - 0.5)^2)^{\frac{\gamma}{2}}$, with $\gamma = 1$, 1.5 and 2. see also [16] and [15]. The computational domain is the same as in the previous examples. The source function $f$ and $u_D$ are manufactured by the exact solution. The diffusion coefficient has been defined to be $\rho = 1$ everywhere. Fig. 6(a) shows the contours of $u_h$ using the values $\gamma = 1$ and $d_g = 0.1$. By this example, we demonstrate the ability of the proposed method to approximate the solution singularities located on the interface of the subdomains with the expected accuracy. We emphasize that the convergence rate is specified by both, the regularity of the solution and the size of the gap. Table 3 displays the expected rates $r$ for several values of the parameters $\gamma$ and $\lambda$. Hence, for validation, we have computed the convergence rates of varying size $d_g = h^\lambda$ and for several values of $\gamma$, which specifies the regularity of the solution, see Table 3. In Fig. 6(b), we plot the convergence rates for $\gamma = 1$ and $\lambda = 1$, 2 and 3. We observe that the rates computed on the last level meshes for $\lambda = 2$ and $\lambda = 3$ confirm the theoretically predicted rates, see Table 3. On the other hand, the rates corresponding to the case $\lambda = 1$ are little higher than the expected. We observe same behavior for the rates plotted in Fig. 6(c) and in Fig. 6(d), which are related to the

cases $\gamma = 1.5$ and $\gamma = 2$. The rates corresponding to $\lambda = 2$ and $\lambda = 3$ are approaching the optimal rates and are in agreement with the theoretical rates. But the rates for $\lambda = 1$ are higher. However, this result can be explained by the "quadratic properties" of the solution on $\partial\Omega_g$. More precisely, the expected rate $r = 0.5$ is coming from the estimate of the first remainder term, see first term in the right hand side in (3.14b) and (3.32). Setting $d_g = h$ in the first term in the right hand side in (3.14b), we get a "continuous quadratic" flux term, whose discrete (second order) analogue term appears in the dG numerical flux formula, see (3.25). In other words, the "quadratic" remainder flux term is implicitly approximated through the numerical flux by second order B-spline space. Hence, the resulting error of the first remainder term, the bound of which is related to the second term in the formula of $\beta$ in Theorem 1, seems to be very weak. The rate that we found is approaching the value $r = 1$ and is the expected value according to the first and third term of the formula of $\beta$, see Theorem 1.

We also study the convergence rates for $\gamma = 0.42$ and $\gamma = 0.38$ which lead to solutions $u$ belonging to $W^{2,1.26}(\Omega)$ and $W^{2,1.23}(\Omega)$, respectively. The convergence rates are plotted in Fig. 6(e) and in in Fig. 6(f), correspondingly. Here, the suboptimal behavior of the rates can be seen for all $\lambda$ cases. Again for the case $\lambda = 1$, the rates are little higher than the expected ones, see first two rows in Table 3. Considering $\lambda = 2$ and $\lambda = 3$, the rates are determined by the regularity of the solution, because the approximation error is of lower order compared to the estimates of the Taylor terms $R_{\Omega_g}$, see the orders $\delta_\Pi(l, p, d)$ and $\beta$ in (4.11). The rates presented in the graphs in Fig. 6(e) and in Fig. 6(f), follow the error bound $\mathcal{O}(h^{\delta_\Pi})$ given in (4.11) and in Table 3.
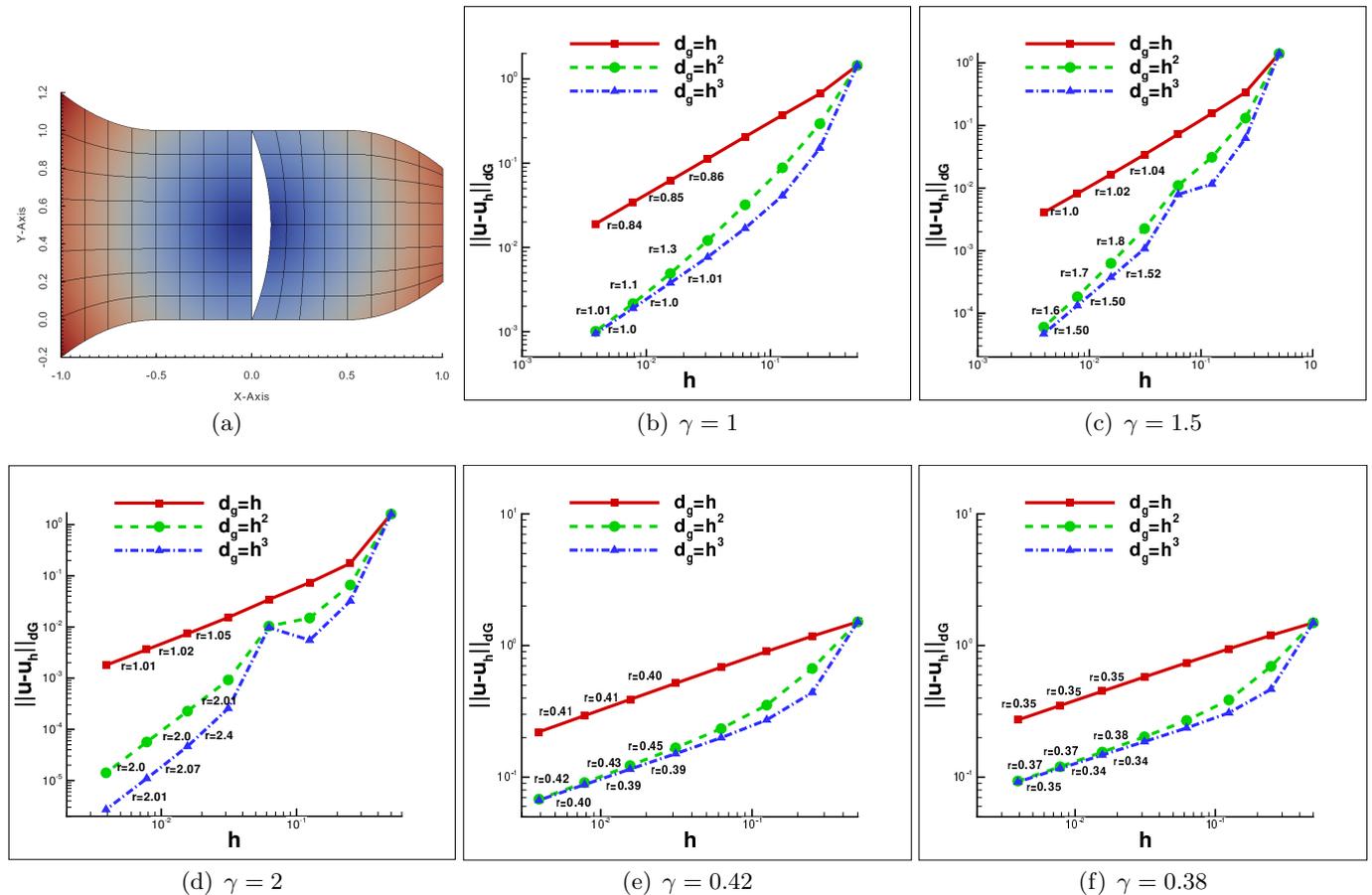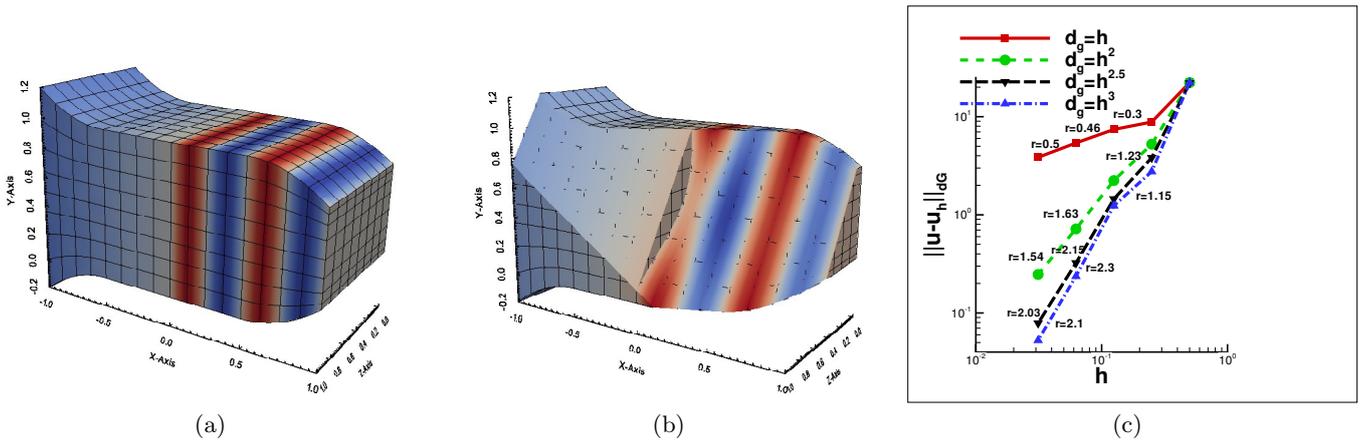


**Fig. 6.** Example 3: (a) The contours of $u_h$ computed setting $\gamma = 1$ and $d_g = 0.1$, (b) convergence rates $r$ for $\gamma = 1$, (c) Convergence rates $r$ for $\gamma = 1.5$, (d) Convergence rates $r$ for $\gamma = 2$, (e) Convergence rates $r$ for $\gamma = 0.42$, (f) Convergence rates $r$ for $\gamma = 0.38$.

## 5.2   Three-dimensional numerical examples

In the three-dimensional tests, the domain $\Omega$ has been constructed by a straight prolongation to the $x_3$-direction of the previous two-dimensional domain. The knot vector in $x_3$-direction is the same as in the other directions, this means $\Xi_i^3 = \{0, 0, 0, 0.5, 0.5, 1, 1, 1\}$ with $i = l, r$. The B-spline parametrizations of the two subdomains have been build by adding a third component to the control points that are listed in Table 1. The third component takes the following values $\{0, 0.25, 0.50, 0.75, 1\}$. Again, the gap region is artificially constructed by moving only the interior control points located at the $x_2 x_3$-plane into the $x_1$-direction.

*Example 4.* Although the first 3d example is a simple extension of the previous two dimensional Example 2, it is still interesting to check the numerical rates. The exact solution is given by (5.1) and the set up of the problem is illustrated in Fig. 7. The interface $F$ is the $x_2 x_3$-plane. In Fig. 7(a), we can see the contours of the solution $u_h$ on both subdomains without having a gap region. Note that the contours resemble the two-dimensional contours along any slice $x_3 = constant$. In Fig. 7(b), we plot the contours of the solution $u_h$ resulting from the solution of the problem in case of having a gap region with $d_g = 0.1$. We can clearly observe the similarities of the contours in Fig. 5(b) and in Fig. 7(b). Also, in Fig. 7(b), we show the shape of the gap as it appears on an oblique cut of the domain $\Omega$. We have computed the convergence rates for the three different values of $\lambda$. The results of the computed rates are plotted in Fig. 7(c). We observe that all the rates are in agreement with the predicted rates by the theory and are similar to the rates of the two-dimensional test Example 2, see Fig. 5(c).



(a)                                    (b)                                    (c)

**Fig. 7.** Example 4: (a) The contours of $u_h$ computed on $\Omega$ , (b) The contours of $u_h$ computed on $\Omega \setminus \overline{\Omega}_g$ with $d_g = 0.1$ , (c) Convergence rates $r$.

*Example 5. $\Phi$-shape gap.* For the second numerical test example, the domain $\Omega$ is the same as in previous example with the subdomain interface $F$ to be the $x_2 x_3$-plane, see Figs. 7(a) and 8(a). We consider a manufactured problem, where the solution is

$$u(x_1, x_2, x_3) = \begin{cases} u_1 := \sin(\pi(x_1 + x_2)) & \text{if } (x_1, x_2, x_3) \in \Omega_1, \\ u_2 := \sin(\pi(4x_1 + x_2)) & \text{if } (x_1, x_2, x_3) \in \Omega_2, \end{cases} \tag{5.2}$$

and the diffusion coefficient is defined to be $\rho_1 = 4$ and $\rho_2 = 1$. We note that, for this test case, we have $[\![u]\!]|_F = [\![\rho \nabla u]\!]|_F = 0$.

Here, we artificially created the gap region such that $\Omega_g \cap \Omega_1 \neq \emptyset$, and consequently for the left gap boundary $F_l$, we get $F_l \neq F$. In particular, in all computations for this example, the two gap parts belonging to $\Omega_1$ and $\Omega_2$ are symmetric with respect to the original interface $F$. In Fig. 8(b), we can see the gap shape for $d_g = 2 \cdot 0.0625$. The contours of the solution $u_h$ computed on a decomposition

with $d_g = 0$ and $d_g = 2 \cdot 0.0625$ are presented in Fig. 8(a) and in Fig. 8(b), respectively. We have computed the convergence rates $r$ for the three different sizes $d_g$ , i.e., $d_g = h^\lambda$ with $\lambda = 1, \lambda = 2$ and $\lambda = 3$. We plot our results in Fig. 8(c). We observe that the rates are approaching the expected values that have been mentioned in Table 2. Furthermore, we note that, for the case $d_g = h$, the rate tends to become 0.5 and is in agreement with the rate predicted by the theory, see Table 2 and Theorem 1. Therefore, in this example, the rates follow the same behavior as in the previous 3d example and do not follow the behavior of the two-dimensional low regularity test case, see Fig. 6.



(a)                                    (b)                                    (c)
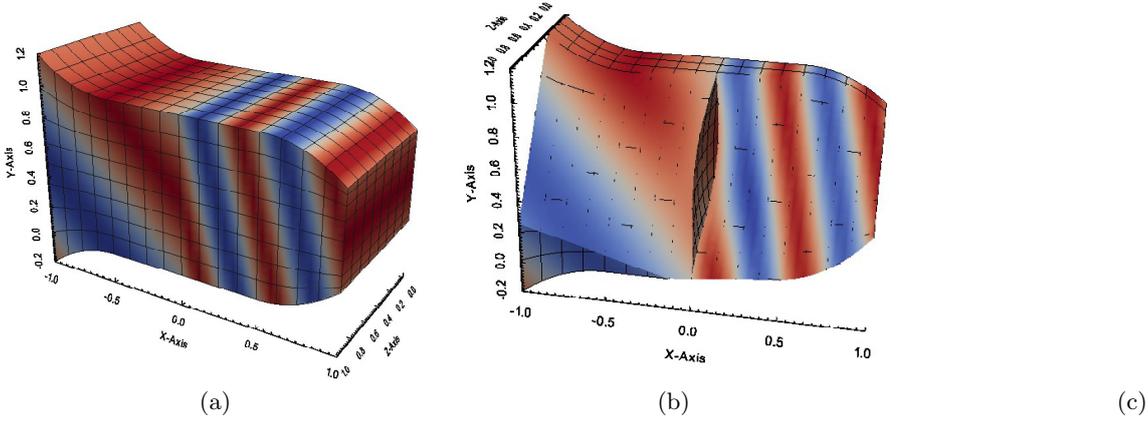
**Fig. 8.** Example 5: (a) The contours of $u_h$ computed on $\Omega$ , (b) The contours of $u_h$ computed on $\Omega \setminus \overline{\Omega}_g$ with $d_g = 2 * 0.0625$ , (c) Convergence rates $r$ for the different $d_g$ sizes.

## 6   Conclusions

In this article, we have developed and analyzed dG IgA methods for discretizing linear, second-order elliptic boundary value problems on volumetric patch decompositions with non-matching interface parametrizations, which include gap regions between the adjacent subdomains (patches). Starting from the original weak formulation, we derived a consistent variational problem on a decomposition without including the gap region. The unknown normal fluxes on the gap boundary were approximated via Taylor expansions. These approximations were adapted to the proposed dG IgA scheme, and the communication of the discrete solution of the adjacent subdomains was ensured. A priori error estimates in the dG-norm $\|.\|_{dG}$ were shown in terms of the mesh-size $h$ and the gap distance $d_g$. The estimates were confirmed by solving several two- and three-dimensional test problems with known exact solutions.

The techniques presented here for linking the diametrically opposite points on the gap boundary can be used for a wide variety of other problems with different gap shapes. The only information, which is required, is the construction of parametrization between the opposite gap boundary parts. This parametrization can be used in conjunction with the Taylor expansions to derive approximations of the normal fluxes on the gap boundary and then to incorporate the numerical fluxes into the dG IgA scheme. From a practical point of view, it would be valuable to derive a posteriori error estimates with computable upper bounds. The functional a posteriori error estimation technique introduced by S. Repin would be one possible method to drive such estimates , see, e.g., [21]. Fast generation techniques for the IgA system matrix and fast parallel solvers for large-scale systems of dG IgA equations are certainly other hot research topics. Fast generation techniques can be constructed on the basis of low-rank tensor approximations as proposed in [**?**]. Efficient solvers can certainly be

constructed on the basis of multigrid, multilevel, and domain decomposition methods. In particular, IETI-DP methods, introduced in [13] and analysed in [10], see also [4, 17] for related BDDC methods, seems to be well suited for the parallel solution of dG IgA equations including the dG IgA schemes studied in this paper.

## Acknowledgments

## References

1. R. A. Adams and J. J. F. Fournier. *Sobolev Spaces*, volume 140 of *Pure and Appled Mathematics*. ACADEMIC PRESS-imprint Elsevier Science, second Edition edition, 2003.
2. A. Apostolatos, R Schmidt, R. Wüchner, and K. U. Bletzinger. A Nitsche-type formulation and comparison of the most common domain decomposition methods in isogeometric analysis. *Int. J. Numer. Meth. Engng*, 97:473–504, 2014.
3. Y. Bazilevs, L. Beir ao da Veiga, J. A. Cottrell, T.J.R. Hughes, and G. Sangalli. Isogeometric analysis: approximation, stability and error estimates for $h$-refined meshes. *Math. Mod. Meth. Appl. Sci.*, 16(7):1031–1090, 2006.
4. L. Beirão Da Veiga, D. Cho, L.F. Pavarino, and S. Scacchi. BDDC preconditioners for isogeometric analysis. *Math. Models Methods Appl. Sci.*, 23(6):1099–1142, 2013.
5. E. Brivadis, A. Buffa, B. Wohlmuth, and L. Wunderlich. Isogeometric mortar methods. *Computer Methods in Applied Mechanics and Engineering*, 284(0):292 – 319, 2015. Isogeometric Analysis Special Issue.
6. J. A. Cotrell, T.J.R. Hughes, and Y. Bazilevs. *Isogeometric Analysis, Toward Integration of CAD and FEA*. John Wiley and Sons, 2009.
7. C. De-Boor. *A Practical Guide to Splines*, volume 27 of *Applied Mathematical Science*. Springer, New York, revised edition edition, 2001.
8. M. Dryja. On discontinuous Galerkin methods for elliptic problems with discontinuous coefficients. *Comput. Meth. Appl. Math.*, 3(1):76–85, 2003.
9. A. Ern and J.-L. Guermond. *Theory and Practice of Finite Elements*, volume 159 of *Applied Mathematical Sciences*. Springer-Verlag New York, 2004.
10. C. Hofer and U. Langer. Dual-primal isogeometric tearing and interconnecting solvers for large-scale systems of multipatch continuous Galerkin IgA equations. RICAM-Report 44, Johann Radon Institute for Computational and Applied Mathematics, Austrian Academy of Sciences, 2015. available at http://www.ricam.oeaw.ac.at/files/reports/15/rep15-44.pdf.
11. T.J.R. Hughes, J. A. Cottrell, and Y. Bazilevs. Isogeometric analysis : CAD, finite elements, NURBS, exact geometry and mesh refinement. *Comput. Methods Appl. Mech. Engrg.*, 194:4135–4195, 2005.
12. B. Jüttler, M. Kapl, D.-M. Nguyen, Q. Pan, and M. Pauley. Isogeometric segmentation: The case of contractible solids without non-convex edges. *Computer-Aided Design*, 57:74–90, 2014.
13. S. Kleiss, C. Pechstein, B. Jüttler, and S. Tomar. IETI–isogeometric tearing and interconnecting. *Computer Methods in Applied Mechanics and Engineering*, 247:201–215, 2012.
14. U. Langer, A. Mantzaflaris, S.E. Moore, and I. Touloupoulos. Mesh grading in isogeometric analysis. *Computers and Mathematics with Applications*, 70(7):1685–1700, 2015.
15. U. Langer, A. Mantzaflaris, St. E. Moore, and I. Touloupoulos. Multipatch discontinuous Galerkin isogeometric analysis. In B. Jüttler and B. Simeon, editors, *Isogeometric Analysis and Applications IGAA 2014*, volume 107 of *Lecture Notes in Computer Science*, pages 1–32, Heidelberg, 2015. Springer.
16. U. Langer and I. Touloupoulos. Analysis of multipatch discontinuous Galerkin IgA approximations to elliptic boundary value problems. *Computing and Visualization in Science*, 17(5):217–233, 2015.
17. L.Beirão Da Veiga, L.F. Pavarino, S. Scacchi, O.B. Widlund, and S. Zampini. Isogeometric BDDC preconditioners with deluxe scaling. *SIAM J. Sci. Comput.*, 36(3):a1118–a1139, 2014.
18. D.-M. Nguyen, M. Pauley, and B. Jüttler. Isogeometric segmentation. part ii: On the segmentability of contractible solids with non-convex edges. *Graphical Models*, 76:426–439, 2014.
19. V. P. Nguyen, P. Kerfriden, M. Brino, S. P. A. Bordas, and E. Bonisoli. Nitsche's method for two and three dimensional NURBS patch coupling. *Computational Mechanics*, 53(6):1163–1182, 2014.
20. M. Pauley, D.-M. Nguyen, D. Mayer, J. Speh, O. Weeger, and B. Jüttler. The isogeometric segmentation pipeline. In B. Jüttler and B. Simeon, editors, *Isogeometric Analysis and Applications IGAA 2014*, Lecture Notes in Computer Science, Heidelberg, 2015. Springer. to appear, also available as Technical Report no. 31 at http://www.gs.jku.at.
21. S. Repin. *A Posteriori Estimates for Partial Differential Equations*. Radon Series on Computational and Applied Mathematics 4, Walter de Gruyter, Berlin, 2008.
22. B. Riviere. *Discontinuous Galerkin methods for Solving Elliptic and Parabolic Equations*. SIAM, Society for industrial and Applied Mathematics Philadelphia, 2008.
23. M. Ruess, D. Schillinger, A. I. Özcan, and E. Rank. Weak coupling for isogeometric analysis of non-matching and trimmed multi-patch geometries. *Computer Methods in Applied Mechanics and Engineering*, 269(0):46 – 71, 2014.
24. L. L. Schumaker. *Spline Functions: Basic Theory*. Cambridge, University Press, third Edition edition, 2007.